QUARTERLY JOURNAL OF THE ROYAL METEOROLOGICAL SOCIETY
*Q. J. R. Meteorol. Soc.* **135**: 1586–1602 (2009)
Published online 28 July 2009 in Wiley InterScience
(www.interscience.wiley.com) DOI: 10.1002/qj.452

# Lagrangian simulation of wind transport in the urban environment

J. D. Wilson[a]*, E. Yee[b], N. Ek[c] and R. d'Amours[c]

[a]*Department of Earth and Atmospheric Sciences, University of Alberta, Edmonton, Alberta, Canada*
[b]*Defence R&D Canada–Suffield, Medicine Hat, Alberta, Canada*
[c]*Canadian Meteorological Centre, Dorval, Quebec, Canada*

**ABSTRACT:** Fluid element trajectories are computed in inhomogeneous urban-like flows, the needed wind statistics being furnished by a Reynolds-averaged Navier–Stokes (RANS) model that explicitly resolves obstacles. Performance is assessed against pre-existing measurements in flows ranging from the horizontally uniform atmospheric surface layer (no buildings), through regular obstacle arrays in a water-channel wall shear layer, to full-scale observations at street scale in an urban core (the Oklahoma City tracer dispersion experiment Joint Urban 2003). Agreement with observations is encouraging, e.g. for an Oklahoma City tracer trial in which sixteen detectors reported non-zero concentration, modelled concentration lies within a factor of two of the corresponding observation in nine cases (FAC2 = 56%). Although forward and backward simulations offer comparable fidelity relative to the data, interestingly they differ (by a margin far exceeding statistical uncertainty) wherever trajectories from source to receptor traverse regions of abrupt change in the Reynolds stress tensor.


KEY WORDS air quality; diffusion; urban dispersion; Lagrangian stochastic model; Langevin model; source-receptor relationship

*Received 9 December 2008; Revised 1 May 2009; Accepted 5 May 2009*

## 1. Introduction

Lien *et al.* (2007) have described the coupling of the Canadian Meteorological Centre's (CMC) Global Environmental Multi-scale weather analysis/prediction model (GEM) and a high-resolution Reynolds-averaged Navier–Stokes (RANS) model of urban winds (urbanSTREAM–Lien and Yee, 2004; Yee *et al.,* 2007; Wang *et al.,* 2009). The latter uses $k-\epsilon$ closure, is provided a detailed three-dimensional (3D) database of building layout, and by virtue of its coupling to regional GEM (via intermediate cascades to 2.5, 1 and 0.25 km grids) may be provided with model fields of the ambient meteorology at a resolution of 250 m–on the basis of which urbanSTREAM performs a detailed computation (gridlength of order metres) of the urban winds. The purpose of this paper is to document the promising performance of a particle trajectory model (urbanLS) that is 'driven' by the wind statistics provided by urbanSTREAM. Trajectories are computed using the well-mixed, 3D Lagrangian stochastic (LS) model of Thomson (1987); novelty here stems from the origin and complexity of the gridded wind field provided to the LS model, from details pertaining to discretization, but primarily in a demonstration of the overall performance of this suite of models.

Being founded on fully 3D velocity statistics, the present modelling approach is valid across a wide range of urban scales, embracing the street canyon scale to the neighbourhood scale. This is distinct from the approach exemplified by Rotach *et al.* (2004) (also Rotach, 2001), whose Lagrangian stochastic model is based on velocity statistics that vary with height alone; the flow field of Rotach *et al.* defines a generic urban roughness layer, and simulates urban dispersion on the neighbourhood scale without resolving buildings. One may classify earlier efforts on the simulation of trajectories in 3D flow according to the following criteria: is the flow *rural* (e.g. Carvalho *et al.,* 2002, who used the Regional Atmospheric Modeling System (RAMS) mesoscale weather model to provide spatially varying velocity statistics to the Lagrangian stochastic model; Mayer *et al.,* 2008, whose trajectory model was driven by the German LMK weather model), or *urban*? Here focusing on the urban case, does the study concern the building or street scale (perhaps flow around a single building), or the neighbourhood scale? Are the 3D velocity statistics computed (e.g. Näslund *et al.,* 1994; Diehl *et al.,* 2007), or measured (e.g. Leuzzi and Monti, 1998), or provided by a heuristic empirical strategy (e.g. Lanzani and Tamponi, 1995; Kaplan and Dinar, 1996; Tinarelli *et al.,* 2007)? Is *fidelity* the primary modelling objective, or are short cuts such as adoption of a simple, heuristic trajectory model (often the Langevin equation: Borrego *et al.,* 2003; Santiago and Martín, 2008) taken in the interest of computational rapidity? Although broadly related to all of the above efforts (and many others we have not cited), the present work is in effect a further (and rather obvious) step down the path

*Correspondence to: Dr J. D. Wilson, Department of Earth & Atmospheric Sciences, 1-26 Earth Sciences Building, University of Alberta, Edmonton, Alberta, Canada T6G 2E3. E-mail: jaydee.uu@ualberta.ca

initiated by Näslund *et al.* (1994) and Lee and Näslund (1998), who simulated dispersion around one or two isolated buildings using (as here) Thomson's well-mixed LS trajectory model, and (as here) providing the needed flow statistics by way of a RANS $k-\epsilon$ calculation.

## 2. Details of the Lagrangian dispersion model

Let $X_i(t)$ be the evolving position of a fluid element and let $U_i(t)$ be the deviation of its velocity from the local mean velocity $\overline{u}_i$, where the latter is a function $\overline{u}_i = \overline{u}_i(\mathbf{x})$ of the coordinate $\mathbf{x} = (x, y, z)$. A first-order LS dispersion model computes the paths of fluid elements by a sequence of discrete time ($\mathrm{d}t > 0$) and distance steps

$$\mathrm{d}X_i = (U_i + \overline{u}_i)\,\mathrm{d}t\,, \tag{1}$$

during each of which the Lagrangian velocity fluctuation evolves according to an Ito stochastic differential equation (or generalized Langevin equation)

$$\mathrm{d}U_i = a_i \mathrm{d}t + b_{ij}\mathrm{d}\xi_j\,. \tag{2}$$

In Equation (2) we can identify a 'memory' term involving the conditional mean acceleration $a_i = a_i(U_i, X_i)$ (here assumed stationary, i.e. having no explicit dependence on time), and a random forcing term responsible for the idiosyncracy of individual paths of the (needed) ensemble. Each component of the random forcing vector $\mathrm{d}\xi_j$ is a Gaussian random variate with $\langle \mathrm{d}\xi_j \rangle = 0$ and $\langle \mathrm{d}\xi_i\,\mathrm{d}\xi_j \rangle = \mathrm{d}t\,\delta_{ij}$ (thus, $\mathrm{d}\xi_i$ is an increment of the Wiener process; Gardiner, 2004). Following Thomson (1987), if we demand that the coefficient $b_{ij}$ ensure consistency of the LS model with the Kolmogorov similarity principle

$$\langle \mathrm{d}U_i \mathrm{d}U_j \rangle = C_0 \epsilon \mathrm{d}t \delta_{ij}\,, \tag{3}$$

then

$$b_{ij} = \sqrt{C_0\,\epsilon}\;\delta_{ij}\,, \tag{4}$$

where $\epsilon = \epsilon(\mathbf{x})$ is the mean turbulent kinetic energy dissipation rate and $C_0$ is a universal constant. Thomson's well-mixed condition provides a (single) constraint on the vector $a_i$, linking its specification to the (known or hypothesized) probability density function (PDF) of the Eulerian velocity fluctuations.

In general, the PDF for the Eulerian velocity in an urban flow is not expected to be Gaussian. Large eddies shed by tall buildings probably ensure that the transport terms $\partial \overline{u_i' u_j' u_k'}/\partial x_k$ in the Reynolds equations are significant, just as they are in the natural roughness sublayer, and this implies the likelihood of velocity skewness (e.g. $S_w = \overline{w'^3}/\sigma_w^3$, where $\sigma_w$ is the standard deviation of vertical velocity) in some regions; indeed Christen *et al.* (2003) reported large negative skewness of vertical velocity in the lee of a building. Nevertheless, experience has shown (e.g. Flesch and Wilson, 1992) that in a regime of turbulence in which skewness is accompanied by drastic *inhomogeneity* of velocity statistics, the latter factor dominates the former at large travel times/distances from the source. This is because differential advection due to strong multi-axial shear in the mean wind field is the (asymptotically) dominant contribution to particle dispersion. Therefore we adopt the approximation that the Eulerian velocity-fluctuation PDF in the urban wind regime is Gaussian, viz.

$$g_a\left(\mathbf{u}'\right) = \frac{\sqrt{\det\left(\mathrm{R}^{-1}\right)}}{(2\pi)^{3/2}}\,\exp\left[-\frac{1}{2}\,u_i'\,R_{ij}^{-1}\,u_j'\right], \tag{5}$$

where dependence on position arises through the spatial variation of the (inverse) of the stress tensor $R_{ij}$. Thomson gave one particular well-mixed LS model[†] that is consistent with Gaussian turbulence, viz.

$$\begin{aligned} a_i = {} & \frac{1}{2}\,\frac{\partial R_{i\ell}}{\partial x_\ell} - \frac{1}{2}\,C_0\,\epsilon\,R_{ij}^{-1}\,U_j \\ & + \frac{1}{2}\,R_{\ell j}^{-1}\,\frac{\partial R_{i\ell}}{\partial x_k}\left(U_j\,\overline{u}_k + U_j\,U_k\right). \end{aligned} \tag{6}$$

The first term is a constant, depending only on the spatial gradient of the Reynolds stress. Remaining terms are either linear or quadratic in the fluctuation $U_i$. Thus symbolically

$$a_i = T_i^0 + T_{ij}^1\,U_j + T_{ijk}^2\,U_j\,U_k\,, \tag{7}$$

(the $T$s are prescribed below).

Thomson's model (Equation (6)) is only one of a class of acceptable models selected by the well-mixed constraint for multi-dimensional Gaussian turbulence. Nevertheless, it has the merit that it does not produce artificial rotation of particle trajectories (Wilson and Flesch, 1997; Sawford, 1999) and no study to date has proven that any alternative model provides a superior simulation of dispersion in highly inhomogeneous turbulence. Sawford (1999) stated that 'until further progress is made, we recommend Thomson's model since it is the simplest'. Näslund *et al.* (1994) and Lee and Näslund (1998) used the Thomson model in what appears to have been the earliest application of the Lagrangian stochastic approach to a (building-resolving) urban dispersion problem: they adopted the standard $k-\epsilon$ turbulence closure in a finite-element discretization to compute the mean flow and turbulent kinetic energy (TKE, $k$) about an idealized rectangular building, and provided these fields to 'drive' zeroth-order and first-order LS models. The model described here differs little from Näslund *et al.,* however we apply it in a much more complex regime of buildings, and thereby are able to extract some insight that may be novel.

[†]Thomson actually gave the equivalent model for the total Lagrangian velocity. The distinction between a model for the increment in Lagrangian *fluctuation* $U_i$ and a model for the increment in *total* velocity $U_i + \overline{u}_i$ can be inferred from

$$\mathrm{d}\left(U_i + \overline{u}_i\right) \equiv \mathrm{d}U_i + \mathrm{d}\overline{u}_i = \mathrm{d}U_i + \left(\overline{u}_j + U_j\right)\mathrm{d}t\,\frac{\partial \overline{u}_i}{\partial x_j}.$$

The drift term in a model for the Lagrangian fluctuation differs from the drift term for a model of the step in total velocity, by the amount $(\overline{u}_j + U_j)\mathrm{d}t\,\partial\overline{u}_i/\partial x_j$.



DOI: 10.1002/qj

### 2.1. Backward simulations

In backward (b) simulations, we retain a positive timestep ($\mathrm{d}t > 0$). Let

$$\begin{aligned} \mathrm{d}X_i^{\mathrm{b}} &= X_i^{\mathrm{b}}(t - \mathrm{d}t) - X_i^{\mathrm{b}}(t) \,, \\ \mathrm{d}U_i^{\mathrm{b}} &= U_i^{\mathrm{b}}(t - \mathrm{d}t) - U_i^{\mathrm{b}}(t) \,, \end{aligned} \tag{8}$$

be the increments one *adds* to particle position and velocity fluctuation, in order to take one computational step further along the backward path. Then

$$\begin{aligned} \mathrm{d}X_i^{\mathrm{b}} &= -\left[\, \overline{u}_i\{\mathbf{X}^{\mathrm{b}}(t)\} + U_i^{\mathrm{b}}(t) \,\right] \mathrm{d}t \,, \\ \mathrm{d}U_i^{\mathrm{b}} &= a_i^{\mathrm{b}}\, \mathrm{d}t + \sqrt{C_0\,\epsilon}\; \mathrm{d}\xi_i \,, \end{aligned} \tag{9}$$

where the conditional mean acceleration (drift coefficient) differs from that given above for the forward model. (Note that, since the random forcing term is Gaussian, the sign attached to the scaling coefficient $\sqrt{C_0\,\epsilon}$ is irrelevant; in other words, the statistics of the processes $\mathrm{d}\xi_i$ and $-\mathrm{d}\xi_i$ are identical, and cannot be distinguished from each other.) Recall that for the forward model the conditional mean acceleration is (merely re-writing Equation (6), with an added superscript f to clarify that this is for application in forward simulations)

$$\begin{aligned} a_i^{\mathrm{f}} = {} & \frac{1}{2}\,\frac{\partial R_{i\ell}}{\partial x_\ell} - \frac{1}{2}\,C_0\,\epsilon\,R_{ij}^{-1}\,U_j \\ & + \frac{1}{2}\,R_{\ell j}^{-1}\,\frac{\partial R_{i\ell}}{\partial x_k}\,\left(U_j\,\overline{u}_k + U_j\,U_k\right), \end{aligned} \tag{10}$$

in which we distinguish terms as being either 'constant' (in the sense of being independent of the Lagrangian velocity fluctuation $U_i$), linear, or quadratic in $U_i$. For backward simulations, instead

$$\begin{aligned} a_i^{\mathrm{b}} = {} & -\frac{1}{2}\,\frac{\partial R_{i\ell}}{\partial x_\ell} - \frac{1}{2}\,C_0\,\epsilon\,R_{ij}^{-1}\,U_j \\ & - \frac{1}{2}\,R_{\ell j}^{-1}\,\frac{\partial R_{i\ell}}{\partial x_k}\,\left(U_j\,\overline{u}_k + U_j\,U_k\right), \end{aligned} \tag{11}$$

where (in effect) all terms emerging from the $\phi/g_a$ term of the Thomson model (i.e. all terms except the classical 'Langevin' damping term) have had their signs reversed. Accordingly, one may unify the code for forward and/or backward simulations by adopting Equation (7) with the $T$s specified as

$$\begin{aligned} T_i^0 &= (-1)^n\,\frac{1}{2}\,\frac{\partial R_{i\ell}}{\partial x_\ell} \,, \\ T_{ijk}^2 &= (-1)^n\,\frac{1}{2}\,R_{\ell j}^{-1}\,\frac{\partial R_{i\ell}}{\partial x_k} \,, \\ T_{ij}^1 &= -\frac{1}{2}\,C_0\,\epsilon\,R_{ij}^{-1} + T_{ijk}^2\,\overline{u}_k \,, \end{aligned} \tag{12}$$

where

$$n = \begin{cases} 0 & \text{forward,} \\ 1 & \text{backward.} \end{cases}$$

Note that, in a horizontally homogeneous and neutrally stratified atmospheric surface layer, terms distinguishing the conditional mean acceleration in forward and backward models vanish.

*Terminology*: simulations will be labelled '1f' or '1b', where '1' signifies the first-order Lagrangian stochastic model as distinct from the zeroth-order ('random displacement') model of section 5.3.

### 2.2. Velocity decorrelation time-scales

In Equation (7) the coefficient $T_{ij}^1$ has the character of an 'inverse time-scale' matrix for relaxation of the velocity fluctuations towards zero: its three eigenvalues imply three time constants. It is helpful for what follows to briefly consider the special case of a stationary flow in which not only is the Eulerian velocity PDF Gaussian, but also independent of position–restrictions which do not conflict with an idealized description of the horizontally homogeneous and neutrally stratified atmospheric surface layer (NSL) as a constant stress layer. For this 'reference flow', Thomson's LS model simplifies drastically. Assuming the $x$-axis is aligned with the mean wind and the friction velocity is defined as $u_* = \sqrt{-\overline{u'w'}} = \text{constant}$, the inverse stress tensor is

$$\mathbf{R}^{-1} = \frac{1}{\sigma^2}\,\begin{pmatrix} \sigma_w^2 & 0 & u_*^2 \\ 0 & \sigma^2\sigma_v^{-2} & 0 \\ u_*^2 & 0 & \sigma_u^2 \end{pmatrix}, \tag{13}$$

where $\sigma^2 \equiv \sigma_u^2\sigma_w^2 - u_*^4$, and the eigenvalues of $T_{ij}^1$ imply three time-scales

$$\begin{aligned} T_L^1 &= \frac{2}{C_0\,\epsilon}\,\frac{2\sigma^2}{\sigma_u^2 + \sigma_w^2 - \sqrt{\left(\sigma_u^2 - \sigma_w^2\right)^2 + 4u_*^4}} \,, \\ T_L^2 &= \frac{2}{C_0\,\epsilon}\,\sigma_v^2 \,, \\ T_L^3 &= \frac{2}{C_0\,\epsilon}\,\frac{2\sigma^2}{\sigma_u^2 + \sigma_w^2 + \sqrt{\left(\sigma_u^2 - \sigma_w^2\right)^2 + 4u_*^4}} \,. \end{aligned} \tag{14}$$

Upon the further simplification $u_* = 0$ (i.e. velocity covariance non-existent or neglected) the time-scales reduce to $T_L^{(1,2,3)} = 2(\sigma_u^2, \sigma_v^2, \sigma_w^2)\,(C_0\,\epsilon)^{-1}$, and give the decorrelation time-scales of three independent Langevin equations for independent velocity fluctuations on the three axes (see also Tennekes, 1979). We henceforth drop the superscript on $T_L^3$, and regard

$$T_L = 2\sigma_w^2\,(C_0\,\epsilon)^{-1} \tag{15}$$

as generally *the* velocity autocorrelation time-scale, relative to which the time step $\mathrm{d}t$ must be limited.

### 2.3. The discretized LS model (implementation)

When an LS model is 'driven' by a computed field of wind statistics, continuous properties (e.g. the mean



DOI: 10.1002/qj

velocity $\overline{u}_i$ and its derivatives $\partial\overline{u}_i/\partial x_j$) are available only at discrete points. The present model (urbanLS) imports a rectangular (Cartesian) grid and accompanying flow field from the building-resolving $k-\epsilon$ model urbanSTREAM. Grid nodes are indexed (I,J,K) where the $x$-axis points eastward, the $y$-axis northward, the $z$-axis vertically, and I = J = 1 labels the southwest corner of the domain. The dimensions of the grid cells are stretched away from the region of interest (urban core) and cells that fall within buildings are distinguished by the logical variable $\gamma$(I, J, K), unity for air space and zero for building space.

For computational efficiency, the unvarying tensor coefficients of Equation (12), i.e. the $T$s, are computed at each grid point and stored for look-up during the trajectory calculations: the $T$s are *not* interpolated from the gridpoints to the particle position, because such a strategy is expensive in terms of computation time, and earlier work (Wilson and Yee, 2000) did not suggest it results in a gain in accuracy (though of course this latter point must depend on the fineness of the flow grid in relation to the inhomogeneity of the velocity statistics).

As indicated above, the core of urbanLS is a standard algorithm for paths of marked fluid elements in turbulence, and novelty arises only from the necessity to evade buildings. Velocity statistics in cells that are adjacent to walls can be regarded as (at best) a reasonable first approximation to reality (urbanSTREAM uses the standard 'wall function' approach to imposition of boundary conditions). However the (actual) variation of the velocity statistics along the path of a particle to a wall is unresolved, so whatever boundary treatment is imposed, it is a parametrization. Obviously one needs some form of (perfect) reflection strategy, which will accomplish the one outcome that is indisputably required: that there be no flux from air space to/from building space. Beyond that requirement, probably the only criterion for treatment of interaction of paths with walls is that it should be such as to ensure particles do not spuriously concentrate near walls, i.e. that the treatment should uphold the well-mixed condition.

The approach that has been taken here is as follows: if, having stepped forward from position $(X_1, Y_1, Z_1)$ in cell (I,J,K) over a distance $(\mathrm{d}X, \mathrm{d}Y, \mathrm{d}Z)$, a particle is found to be in an illegal cell ($\gamma = 0$), then it is reflected off the *first* solid wall it would have encountered along its path. It is placed at an arbitrary distance $\ell_n$ ('nudging distance'; $\ell_n = 1$ m for the Oklahoma City simulations) outside the wall, with its velocity fluctuation randomly reset, i.e.

$$U_i = \sigma_{(i)}\, r_{(i)} \tag{16}$$

(where the $r_i$ are independent standardized Gaussian random variables; the brackets $(i)$ indicate summation is not to be applied). In some wall-adjacent cells, the computed flow field may have the peculiarity that the mean velocity vector drives a particle into a crevice (junction of two building walls), while the (computed) velocity standard deviation is insufficiently large to ensure a prompt escape. (Such cells are labelled 'inescapable' according to a criterion on the turbulence intensity.) The consequence is that a particle may encounter a solid wall after having made a distance step that is arbitrarily small, and indeed may cross two or more walls simultaneously. The logic required to deal with all possibilities is taxing, not to mention computationally laborious, and so the subroutine involved very occasionally does fail to prevent entry into a building. The approach taken is to tolerate this (extremely rare) outcome, and merely abandon the particle in question whether or not the offending step was launched from an 'inescapable' cell. This is a concession to the requirement that the code be robust. A further concession relates to the numerical instability of Thomson's model examined by Yee and Wilson (2007): except where otherwise noted, rather than incorporate their semi-analytical time integration which eliminates the instability, the present version of urbanLS uses ordinary Cauchy–Euler time-stepping (Gardiner, 2004), and should the velocity fluctuation exceed $n$ (= 6 here) times the local standard deviation, the velocity is reset in accordance with Equation (16).

We have covered the basic principles of the LS model. Any number of steady (or transient) sources may be specified, and for each one a large ensemble of paths is computed (this being sub-divided into sub-ensembles, so that a standard error may be attached to any computed statistic of the concentration field) to any number of detectors. Regarding the latter, a subroutine makes a careful (but laborious) assignment of the contributions of particle residence time in each user-specified detector (these are rectangular, and specified by their centre position and half-span on each axis), whereas every grid cell also functions as (rapid, but less exact) detector, in that a residence time contribution d$t$ is added to the cell occupied by a particle at the end of its step. As a detail not relevant to the tracer gas simulations shown here, a particle size distribution may be specified, and a partial reflection probability (off ground and buildings) can be computed following Wilson *et al.* (1989).

### 2.4. Specification of the Kolmogorov constant $C_0$

Free specification of the (nominally universal) Kolmogorov coefficient $C_0$ amounts to 'tuning' the Lagrangian model, which (objectivity demands) should be done once and for all, relative to best available *relevant* observations. Although inessential, it is informative to interpret the tuning of $C_0$ in the context of the following subtle (and inexact) argument – that the value adopted for $C_0$ correlates with the (implied) specification of an effective turbulent Schmidt number, i.e. ratio $S_c = \nu_T/K$ of the eddy viscosity to the eddy diffusivity for mass, in an (implicit, hypothetical) eddy diffusion treatment.

To put this idea in context, we note that in broad terms a 'diffusion' treatment of turbulent convection is plausible to the extent that a particle's cumulative displacement from its point of release can be regarded as being the sum of many independent random distance steps; the 'far field' of a source is by definition the



DOI: 10.1002/qj

regime (in time or distance from release) where this is true. Accordingly, reconciliation of the Lagrangian stochastic and eddy diffusion treatments (in the far field) has been a familiar theme since Taylor (1921); and Durbin (1983) proposed as a criterion for generalized Langevin (or first-order Lagrangian stochastic) models that they should reduce, in the limit of vanishing velocity autocorrelation time-scale $T_L$ (or in practice, if the ratio $t/T_L$ of travel time to time-scale is very large), to an equivalent random displacement model (RDM, or 'zeroth-order LS model'), i.e. to a stochastic equation for increments in particle position. Focusing on vertical dispersion, in view of Equation (15) we may envisage that the 'diffusion limit' of a Langevin model is the RDM implied in the limit of infinite $C_0$ (interpreted as implying $T_L \to 0$, with compensating increase in $\sigma_w$, such that $K = \sigma_w^2 T_L$ is held finite). Amplifying Durbin's idea, Thomson (1987) qualified the circumstances under which a first-order Lagrangian stochastic description of turbulent transport *should* be equivalent to (or imply) a random displacement model: if $\tau_H$ is a time-scale characterizing the inhomogeneity of the turbulence, then what is of immediate interest is Thomson's point that in strongly inhomogeneous turbulence 'it is not clear whether the model becomes an eddy-diffusion model at large times or indeed whether it should'.

Arguably the most suitable observations to tune the present LS model–for they are unambiguous and took place in the simplest regime of surface-layer turbulence–are those of the Project Prairie Grass (PPG) short-range tracer dispersion trials (Barad, 1958; Haugen, 1959) that occurred in neutral stratification. As the source was near ground, dispersion during neutral runs occurred in a regime of turbulence characterized by a nominally height-independent vertical velocity standard deviation $\sigma_w$, and a vertical velocity autocorrelation time-scale (nominally) varying linearly with distance $z$ from ground. A suitable scale for the inhomogeneity of turbulence in this idealized, horizontally homogeneous NSL is

$$\tau_H \equiv \frac{T_L}{\sigma_w}\left(\frac{\partial\, T_L}{\partial z}\right)^{-1} = \frac{z}{\sigma_w}\,. \tag{17}$$

It is easy to show (retrospectively, from what follows below) that for the PPG trials (and for the NSL in general) $\tau_H \sim T_L$, for from the calibration adopted below it follows that $T_L \approx 0.5 z/\sigma_w$. Thus, Thomson's caution applies, that it is not clear whether the first-order LS model implies an eddy diffusion model, or whether it should. However what is certain is that, the eddy viscosity in the NSL being $\nu_T = k_v u_* z$ (where $k_v$ is the von Kármán constant), the far-field eddy diffusivity must be

$$K \equiv \frac{1}{S_c}\, k_v u_* z\,. \tag{18}$$

(This follows by definition of the turbulent Schmidt number, which it is usual to assume is constant across the flow, such that $k_v/S_c$ may be called the 'von Kármán constant for mass'.) As the PPG source was only 0.46 m above ground and the nearest detector was 50 m downwind, the PPG observations lie in the far field of the source. Provided that the effective Schmidt number in Equation (18) is assigned a value $Sc \approx 0.63$, these observations can be quite well reproduced by Eulerian dispersion models,[‡] i.e. by solving the advection–diffusion equation or computing trajectories by means of an equivalent random displacement model.

Recognizing the connection is not rigorous for the reasons covered above, in a heuristic spirit we may extract a value for the Kolmogorov coefficient by reconciling Equation (18) with the eddy diffusivity

$$K^{\text{eff}} = \frac{2\left(\sigma_w^4 + u_*^4\right)}{C_0\,\epsilon} \tag{19}$$

implied (Sawford and Guest, 1988) by the diffusion limit of Thomson's multidimensional LS model for Gaussian turbulence. (Note that, if covariance of along-wind and vertical velocity fluctuations were neglected in the LS model, then implicitly $u_* \to 0$ in Equation (19), but not, of course, in Equation (18)). Equating Equations (18), (19) and invoking the idealization that in the NSL $\epsilon = u_*^3/k_v z$ (i.e. local equilibrium), we find

$$\frac{1}{S_c} = \frac{2}{C_0}\left(c_w^4 + 1\right)\,, \tag{20}$$

where $c_w = \sigma_w/u_* \approx 1 - 1.3$ (Wilson, 2008). If the target value of $S_c$ is regarded as fixed, then the ratio of the optimal values for $C_0$ in LS simulations of the NSL that retain (3D) and neglect (1D) velocity covariance is

$$\frac{C_0^{(3D)}}{C_0^{(1D)}} = \frac{c_w^4 + 1}{c_w^4}. \tag{21}$$

Interestingly Equation (21) is almost (but not quite) identical to the ratio implied by demanding equality (for 1D and multi-dimensional LS simulations of the NSL) of the third of Equations (14) , viz.

$$\frac{C_0^{(3D)}}{C_0^{(1D)}} = \frac{\sqrt{c_u^2 c_w^2 - 1}}{c_w^2}, \tag{22}$$

(where $c_u = \sigma_u/u_*$). With ($c_u = 2$, $c_w = 1.3$) Equation (21) evaluates to 1.35, whereas Equation (22) evaluates to 1.42.

In this paper we adopted Equation (20) and assumed the NSL best characterized by ($c_w = 1.3$, $S_c = 0.63$), on

[‡]Wilson and Yee (2007) found that first-order Lagrangian simulations of Project Prairie Grass tracer dispersion *can* be distinguished from zeroth-order Lagrangian simulations ('Random Displacement Model'), which as noted are equivalent in principle to an Eulerian eddy-diffusion treatment. This is consistent with Thomson's reservation, that if (as is the case in the neutral surface layer) $\tau_H \sim T_L$ then 'it is not clear whether the model becomes an eddy-diffusion model at large times'. The distinction between these two classes of models is anyway not of great practical importance as regards performance for far-field dispersion; however Wilson and Yee argue in favour of the Langevin-type of Lagrangian model on the basis of its wider generality and only marginally lesser computational efficiency.



DOI: 10.1002/qj

the basis of earlier simulations (both Lagrangian and Eulerian) of Project Prairie Grass; results of section 3 confirm this choice. Thus our calibration of Thomson's first-order LS model to reality was achieved by setting the Kolmogorov constant $C_0 = 4.8$ (see also Wilson *et al.,* 2001, Appendix A; Sawford, 2001). From the above reasoning, in any simulation for which velocity covariance is neglected in the LS model (in which case $u_* \to 0$ in Equation 19), one must set $C_0 = 3.59$. Unless otherwise stated, in simulations to be shown velocity correlation was retained.

### 2.5. Rate of horizontal dispersion not calibrated

Thomson's model is configured to reproduce the desired velocity PDF and Kolmogorov structure function (Equation (3)), however it is not tailored to a measured (or hypothetical) power spectrum of velocity (or equivalently, a velocity autocovariance function). As seen earlier, Equation (6) implies comparable decorrelation time-scales for the vertical and horizontal components of velocity, although greater differences (than conveyed by Equations (14)) exist when the restrictions leading to those results are removed, i.e. in the presence of vertical and/or horizontal gradients in velocity statistics. Thus the spectral range of the (model's) horizontal velocity fluctuations is approximately the same as the spectral range of the vertical velocity, the latter tuned (by virtue of the way $C_0$ controls the decorrelation time-scale) against vertical dispersion.

Of course, in principle one *could* have chosen $C_0$ to optimize agreement with the observed rate of *horizontal* spread, e.g. to best conform the model to observed plume cross-wind standard deviation $\sigma_y(x)$ at streamwise distance $x$ from a source. However $\sigma_y(x)$ is (comparatively) ambiguous – or perhaps one should rather state, is sensitive to a greater number atmospheric conditions than is vertical spread. In the surface layer, the power spectrum of vertical velocity is adequately characterized by a single height-varying time-scale, but horizontal velocity spectra typically lack that convenient property. In addition to the rapid variability of the 'active' (stress-carrying) eddies (which the multi-dimensional LS model *does* represent) horizontal velocity spectra may (and usually do) contain a slow component related to the large 'inactive' turbulent eddies of the ABL–and possibly also a contribution from mesoscale motion. In short, particularly in the case (as here) that velocity statistics for the Lagrangian model are furnished by a RANS wind simulation, horizontal velocity fluctuations are not parametrized with the same level of fidelity as are the vertical.

### 2.6. Time step

The graininess of the computed flow field imposes an inhomogeneity length-scale, and for the calculations shown here the time step was specified as

$$\mathrm{d}t = \mu \min\left[T_L,\ \tau_h\right], \quad (\mu \ll 1)\ , \tag{23}$$

where $T_L$ is defined by Equation (15), and the inhomogeneity time-scale

$$\tau_h = \frac{\sqrt{\Delta x_i \Delta x_i}}{\sqrt{(U_i + \overline{u}_i)\ (U_i + \overline{u}_i)}} \tag{24}$$

represents the transit time across a grid cell. Thus distance steps are required to be small with respect to the cell size.

## 3. Demonstration of consistency relative to Project Prairie Grass

With appropriate choice of the Kolmogorov constant $C_0$, the first-order LS model is known to provide an excellent simulation of vertical dispersion in the neutral atmospheric surface layer, as observed in Project Prairie Grass. Recall however that, in the context of its being provided *continuous* profiles of velocity statistics, a Lagrangian model is 'grid free' – whereas this is not an attribute of the present code (urbanLS), which is set up to exploit a gridded field of velocity statistics (that is, the present model is subject to a discretization error that is absent in a model able to represent $\overline{u}$ etc. as continuous functions of position). In a horizontally homogeneous wall shear layer, e.g. the horizontally homogeneous, neutrally stratified atmospheric surface layer ('hhNSL'), the Reynolds stress tensor is spatially invariant. This implies that as a particle moves from cell to cell of the grid (i.e. as its indices change) there are no stepwise variations in the velocity variances and covariances. However the mean velocity $\overline{u}(z)$ and the dissipation rate $\epsilon(z)$, by virtue of the way urbanLS is tied to a flow grid, are discontinuous. Thus we ought not necessarily to expect urbanLS to *exactly* reproduce the solution that would obtain in the case of a non-gridded Lagrangian solution.

Nevertheless the same excellent performance can be demanded of the present gridded implementation, provided the grid is sufficiently fine to provide a suitable resolution of the velocity statistics. To demonstrate this, an ideal, horizontally uniform wall shear layer was overwritten onto urbanSTREAM's grid for the Oklahoma City trial 'IOP9r2' (section 5), velocity statistics being specified as: $\sigma_u/u_* = \sigma_v/u_* = 2$, $\sigma_w/u_* = 1.3$, $\epsilon = u_*^3/(k_v z)$, $\overline{u} = (u_*/k_v)\ \ln(z/z_0)$. The cell centres, $z_c$, of the Oklahoma grid span the height range from $1.4925 \le z_c(K) \le 761.27\,\mathrm{m}$, where $K \ge K_{\min}$ is the cell index. By (arbitrarily) specifying the roughness length as $z_0 = z_c(K_{\min})/2 = 0.74625\,\mathrm{m}$ we can perform an hhNSL simulation from a ground-level source placed (arbitrarily) at $x = 1000\,\mathrm{m}$ on the Oklahoma grid out to a fetch of $5000 z_0$, i.e. a distance of travel of 3.7312 km (taking the particle to $x = 1000 + 3731.2\,\mathrm{m}$ on the grid). By this rescaling of the geometry, we represented the surface-layer (hhNSL) velocity statistics with over 58 grid points in the lowest 200 m ($268 z_0$), thereby limiting the discretization error.

We are concerned to demonstrate the consistency of the trajectory model's predictions of crosswind-integrated concentration $\chi/Q$ with the reference (i.e.



DOI: 10.1002/qj

Table I. Normalized crosswind-integrated concentration $z_0\, u_*\, \chi/(k_v Q)$ at height $z/z_0 \leq 20$ due to a continuous point source near the wall in a wall shear layer, as computed by urbanLS on a discrete flow grid ($19 \times 32\,000$ paths). The symbol ✓indicates that velocity covariance is retained. These results document the need for a small time step ($\mathrm{d}t = \mu\, T_L$), confirm the (expected) forwards/backwards equivalence, and illustrate that the value specified for $C_0$, as indicated by Equation (21), should be harmonious with the decision to include/neglect velocity covariance.

| Forward/backward | $\mu$ | $C_0$ | $S_c$ | $x/z_0$ | PPG | $z_0 u_* \chi/(k_v Q)$ |
|---|---|---|---|---|---|---|
| f | 0.1 | 4.8✓ | 0.63 | 2000 | $1.46 \times 10^{-3}$ | $1.35 \times 10^{-3}$ (0.01) |
| b | 0.1 | 4.8✓ | 0.63 | ·· | ·· | $1.30 \times 10^{-3}$ (0.01) |
| f | 0.02 | 4.8✓ | 0.63 | ·· | ·· | $1.44 \times 10^{-3}$ (0.005) |
| b | 0.02 | 4.8✓ | 0.63 | ·· | ·· | $1.45 \times 10^{-3}$ (0.01) |
| f | 0.02 | 4.8 | 0.84 | ·· | ·· | $1.80 \times 10^{-3}$ (0.01) |
| f | 0.02 | 3.59 | 0.63 | ·· | ·· | $1.42 \times 10^{-3}$ (0.01) |
| f | 0.1 | 4.8✓ | 0.63 | 5000 | $6.0 \times 10^{-4}$ | $5.26 \times 10^{-4}$ (0.05) |
| f | 0.02 | 4.8✓ | 0.63 | ·· | ·· | $5.88 \times 10^{-4}$ (0.06) |
| f | 0.02 | 3.59 | 0.63 | ·· | ·· | $5.68 \times 10^{-4}$ (0.04) |

Tabulated 'true' PPG values are from Wilson (1982b, p412). In brackets, rounded and without multiplier, is the standard error computed from the 19 sub-ensembles. (e.g. row 1: relative error 0.01/1.35).

field-calibrated, or Project Prairie Grass) value. At a dimensionless distance of $|x - x_{\mathrm{src}}|/z_0 = 2 \times 10^3$ from the source and beyond, the crosswind-integrated concentration $\chi/Q$ is almost invariant below $20z_0$ (Wilson, 1982b). For forward simulations the source, treated as a point, was placed at $z = 13.5\,\mathrm{m}$ ($z/z_0 = 18$, i.e. effectively ground level), and trajectories were reflected at $z_{\mathrm{refl}}/z_0 = 1$. The forward detector was centred at $z = 4.5\,\mathrm{m}$ ($z/z_0 = 6$), and had half-spans $(100, 700, 3)\,\mathrm{m}$ in the along-wind, cross-wind and vertical directions. Backward simulations used a point source at the centroid of the crosswind-integrating forward detector, and a crosswind-integrating detector, also with half-spans $(100, 700, 3)\,\mathrm{m}$, whose centroid coincided with the forward point source. The along-wind span of detectors ($\pm 100\,\mathrm{m}$) is small relative to the large dimensional fetch, while the vertical span is negligible in view of the height-constancy of $\chi$ at this low height and large fetch. The wide lateral span of the detectors performs the cross-wind integration.

Table I lists the outcomes of hhNSL simulations in relation to the correct value.[§] Forward and backward simulations show the expected consistency, and provided the time step is sufficiently small (and with a proviso on the specification of $C_0$, see below), agree closely with the observations. It was noted in section 2.4 that in the context of a first-order LS model the Kolmogorov constant $C_0$ is implicitly related to the effective turbulent Schmidt number $S_c$, but that the relationship is ambiguous in the sense that it depends on the dimensionality of the Lagrangian model (and more particularly, the inclusion or otherwise of velocity covariance). That the 'true value' of $C_0$ has proved elusive is well known, and certainly the validity of Equation (20) is quite restricted. However Table I confirms that, if one chooses to eliminate velocity covariance, the constant $C_0$ *does* need to be adjusted (according to Equation (20)) so as to ensure $S_c = 0.63$, the value implied by the neutral PPG data whether one best fits an Eulerian (Wilson, 1982a) or a first-order Lagrangian (Sawford, 2001) model.

Having established what is needed as regards calibration so that short-range atmospheric dispersion in its very simplest manifestation–a surface source in the neutral and horizontally homogeneous surface layer–is satisfactorily simulated, we now examine the performance of urbanLS in complex, urban-type flows.

## 4. Performance relative to observations in water-channel flow: MUST

The Mock Urban Setting Test (MUST) experiments (Yee and Biltoft, 2004) involved an array of shipping containers (12.2 m long by 2.42 m wide by 2.54 m high) laid out to form a regular unstaggered array on a salt flat at the Dugway Proving Grounds, in Utah, USA. Here we examine the performance of the LS model relative to gas dispersion measurements carried out in a water-channel analogue to atmospheric-MUST (Yee *et al.,* 2006; Hilderman and Chong, 2007). The water-channel array (Figure 1) entailed $12 \times 10$ obstacles with dimensions $(X, Y, H) = (11.8,\ 59.4,\ 12.4)\,\mathrm{mm}$, where $x$ is the direction of the mean stream. The canyon widths were $(X_{\mathrm{c}}, Y_{\mathrm{c}}) = (62.9,\ 38.5)\,\mathrm{mm}$ so that the spacing between front faces ($x$-wise periodicity length) was $X + X_{\mathrm{c}} = 74.7\,\mathrm{mm}$ (or $6.024H$).

A computed 3D field of the velocity statistics was provided by the $k - \epsilon$ model urbanSTREAM, measured

[§]The tabulated PPG values from Wilson (1982b), case $\Omega \equiv z_0/L = 0$, can be considered within 5% of the 'true reference value'. (Since field observations in the hhNSL define the true value, and they themselves carry uncertainty, we must regard the true values as uncertain to about this extent, i.e. ±5%.) The tabulated values of Wilson (1982b) were computed with a grid-free, well-mixed 1D LS model (no streamwise and lateral velocity fluctuations, $u'$, $v'$) that had been verified (Wilson *et al.,* 1981; Wilson, 1982a) against the reference data, i.e. neutral dispersion experiments of Project Prairie Grass.



DOI: 10.1002/qj

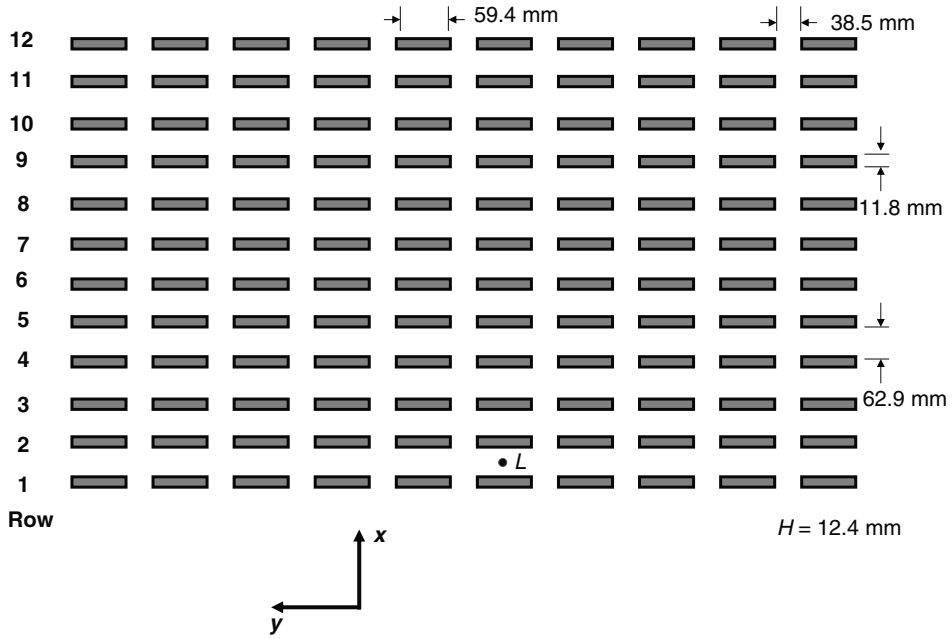


Figure 1. Configuration of the water-channel MUST experiments. The mean flow was directed along the $x$-axis, and the tracer point source was at position **L**. $H = 12.4$ mm is the height of the obstacles.

profiles being imposed at the upstream (inflow) boundary. The computational mesh, imported by the trajectory model along with the velocity statistics, was defined by $202 \times 42 \times 44$ coordinate planes cutting respectively the streamwise ($x$), lateral ($y$) and vertical ($z$) directions, and spanning a volume of $(1.152 \times 0.0979 \times 0.2484)$ m or $(93 \times 8 \times 20)H$. The flow simulation encompassed only a single row of obstacles, and a periodic lateral boundary condition was applied on the cross-wind ($y$) axis, hence the narrow cross-wind extent of the domain. (For trajectory simulations, flow statistics were extrapolated outside the grid by invoking the assumed periodicity along the $y$ axis.) The $x$-coordinate origin lies at the upwind face of the first building, the $y$-origin on the midline of the array, and $z = 0$ on the lower boundary. The dimensions of the computational cell containing the tracer source (position **L** in Figure 1) were $(\Delta x,\ \Delta y,\ \Delta z) = (2.2,\ 2.2,\ 1.13)$ mm.

Figure 2 compares observed and simulated flow fields at the source position **L** (Figures 4 and 5 of Wang *et al.,* 2009 give a more detailed comparison). The flow model gives rather a good simulation of the mean velocity (except in the lee of the building, where it appears to overestimate the magnitude of the–reversed–velocity vector), but discrepancies relative to the measured velocity variance are of the order of 100%. Performance at other locations was comparable. Elsewhere Lien and Yee (2004) examined the performance of this flow model for an array of cubes, i.e. a flow of qualitatively the same nature as the present MUST flow. Again, simulations gave a good streamwise mean velocity field $\overline{u}$, with greatest errors in the recirculation zone behind the obstacle farthest downstream. Largest errors in the mean vertical velocity $\overline{w}$ were of order 25%. The computed TKE field was qualitatively poorer than the mean velocity field, with errors of up to 100% (though typically no worse than 50%).

### 4.1. Simulated versus observed concentration field

A continuous point source of tracer was located at position **L** (Figure 1) between the first and the second row of obstacles, at $\mathbf{x}_{\rm src} = (43.25,\ 0,\ 0.564)$ mm, where the physical source had diameter 2.8 mm and released tracer fluid (a fluorescent dye–water mixture) at volume flow rate $V_s = 12\,\mathrm{ml\,min^{-1}} = 2 \times 10^{-7}\mathrm{m^3 s^{-1}}$ (volume-mean exit-velocity in the exit jet $32\,\mathrm{mm\,s^{-1}}$; the tracer released from the source was rapidly mixed into the wake region of the upwind obstacle, producing effectively a 'volume' source). In the simulations to follow, urbanLS treated the source as a passive point source, and simulated concentrations at the available observation points were insensitive to source placement within the height range $0 \le z_{\rm src} \le H/2$. Mean concentrations will be given as $C/Q$ where $Q\,\mathrm{kg\,s^{-1}}$ is the tracer source strength, and relate to the concentration ratio $C/C_s$ (where $C_s\,\mathrm{kg\,m^{-3}}$ is the concentration of tracer in the tracer–water mixture emanating from the source) according to $C/C_s \equiv V_s\, C/Q$. Trajectories were reflected at $z_{\rm refl} = 2$ mm ($z_{\rm refl}/H = 0.16$).

Simulations of the MUST experiment with time step $\mathrm{d}t/T_L = \mu = (0.02,\ 0.1)$ provided indistinguishable outcomes, and the influence of the velocity covariance was also minor. Due to the reverse mean flow in the lee of the 'buildings', most trajectories from the source progressed against the background (or overhead) flow and towards the leeward wall of the first building; after some meandering, these tracer particles escaped, most often around the sides of the building into the stronger current down



DOI: 10.1002/qj

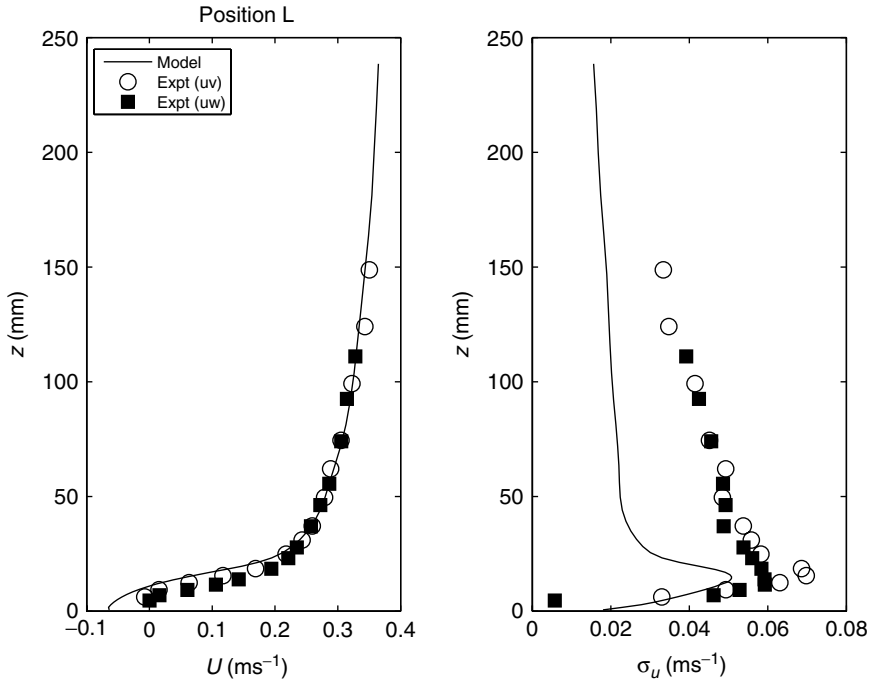


Figure 2. Comparison of urbanSTREAM flow simulation with observations in the water channel MUST flow, for the source position **L**, centred in the canyon in the lee of the first 'building'. Notations (uv) and (uw) denote orientation of laser beams of the laser doppler velocimeter used to measure the specified two velocity components. Note the reverse mean velocities in the urban 'canyon'.

the streamwise-oriented urban 'canyons'. Figure 3 indicates that the predictions of the LS model are not in particularly good accord with the observations. There is a visible offset of the observed plume centreline relative to the computational $y = 0$ axis (about which, supposedly, the water-channel flow exhibited reflection symmetry; we suspect that in reality the water channel flow was imperfect in that regard, as is frequently the case; D. J. Wilson, personal communication). However even if one eliminates that bias, the predicted plume is too narrow, and (in consequence) centreline concentration decays more slowly with increasing downstream distance than the observations. Interestingly, Eulerian simulations[¶] (e.g. Keats *et al.* (2007), Figure 5a) also with $S_c = 0.63$ exhibited the same tendency, and overall, they were of a very similar quality. Knowing that the flow field is imperfectly computed, one is unsure what part of the error indicated by Figure 3 is due to the trajectory model.

### 4.2. Comparison: Forward and backward simulations

To test for the (expected) consistency of forward and backward LS algorithms, a set of simulations were run with the particle release position randomized over a volume whose dimensions exactly matched those of the detectors, the half-spans specifically being $(0.020, 0.005, 0.001)$ m. In a first consistency test, the forward source was centred at position **L** (i.e. between the first and the second row of obstacles at $x = 0.04325$ m, $y = 0$, $z = H/2$), while the forward detectors (for convenience labelled $\mathbf{D}_1, \mathbf{D}_2, \mathbf{D}_3$) were centred at $y = 0, z/H = 1/2$ at downwind positions $x = 0.2$ m (midway between third and fourth buildings), $x = 0.64$ m (midway between ninth and tenth buildings) and $x = 0.86$ m (downwind of the twelfth and final building of the array). The corresponding backward simulations were performed with a (volume) source at each (in turn) of the three ('forward') detector positions ($\mathbf{D}_1, \mathbf{D}_2, \mathbf{D}_3$), and a single ('backward') detector at position **L**. Then (for example) forward and backward simulations would be considered perfectly consistent if the $C/Q$ ratio at $\mathbf{D}_3$ due to the (forward) source at **L** exactly matched the $C/Q$ predicted for position **L** by a backward simulation with (backward) source at position $\mathbf{D}_3$.

Table II indicates that the theoretical forward–backward equivalency of the infinitesimal Thomson model does not (in general) carry over to a discrete implementation, the magnitude of the discrepancy being in some manner proportional to the complexity of the flow region that is sampled by trajectories from source to detector. When the source and detector lie well above the obstacles such that streamwise gradients are weak, forward and backward simulations *are* consistent (backward to forward ratios no more different from unity than can reasonably be

[¶]The Eulerian simulations performed by urbanSTREAM used an isotropic eddy diffusivity $\nu_T/S_c$, and thus that model differed somewhat from urbanLS, which implements whatever anisotropy is implied by the ratio $\sigma_u : \sigma_v : \sigma_w$ in the fields provided; however anisotropy in the turbulence predicted using urbanSTREAM is probably quite small, due to the simple Boussinesq eddy-viscosity approximation used to compute the Reynolds stress tensor. In any case, lateral spread of a plume in a regime of flow like this is dominated by differential advection (e.g. Wilson *et al.,* 1993), and is accordingly less sensitive to specification of the diffusivities for along-stream ($x$) and cross-stream ($y$) spread.



DOI: 10.1002/qj

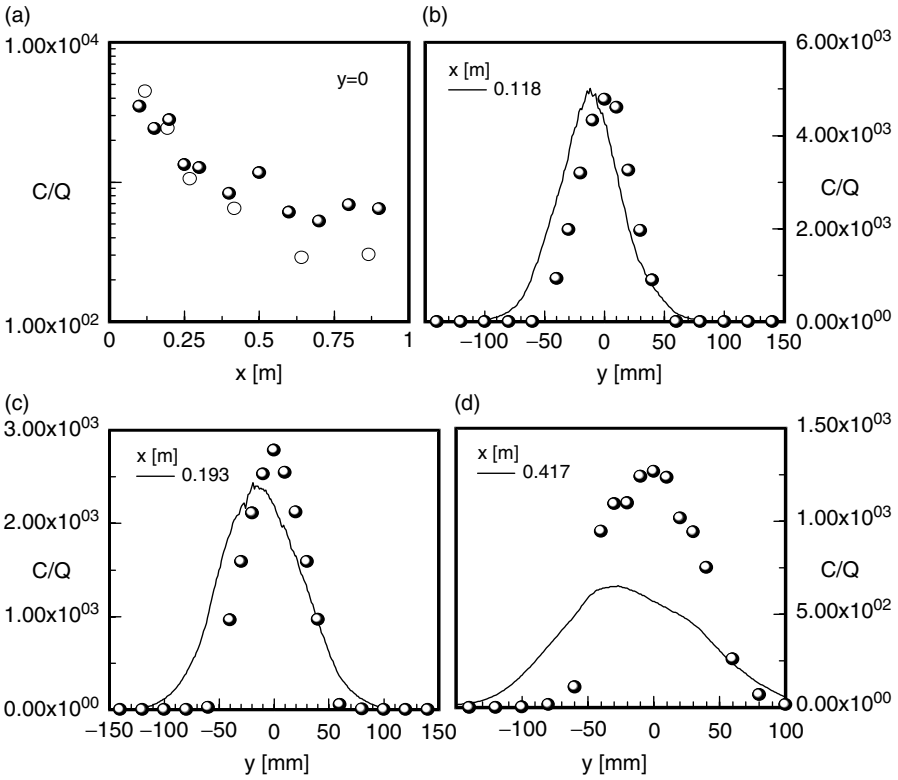


Figure 3. Observed (lines or open circles) and modelled (shadowy points) concentration transects in the water channel MUST array at height $z/H = 1/2$. (a) gives the streamwise transect along $y = 0$, other panels give cross-stream transects (b) midway between second and third buildings (cf. Keats *et al.,* 2007, Figure 5a), (c) midway between third and fourth, and (d) midway between sixth and seventh buildings. The streamwise interval between the upstream faces of successive buildings is $6.024H$.

Table II. Ratios $C_b/C_f$ of mean concentrations from backward and forward simulations of a source in the MUST flow, comparing outcomes using elementary or semi-analytic (s.a.) time-stepping. Volumes of sources and detectors are identical, their heights being (all) $4H$ or (all) $H/2$, where $H = 0.0124$ m is the height of the 'buildings'. The cited statistical uncertainty was computed by adding the relative errors (standard error divided by mean) for forward and backward computations.

| $x$ (m) | $C_b/C_f$ | $C_b/C_f$ (s.a.) |
|---|---|---|
| Source and detectors at $z/H = 4$ | | |
| 0.2 | $1.005 \pm 0.007$ | $0.994 \pm 0.008$ |
| 0.64 | $1.072 \pm 0.030$ | $0.958 \pm 0.029$ |
| 0.86 | $1.044 \pm 0.035$ | $0.980 \pm 0.033$ |
| Source and detectors at $z/H = 1/2$ | | |
| 0.2 | $1.189 \pm 0.018$ | $1.148 \pm 0.021$ |
| 0.64 | $1.333 \pm 0.033$ | $1.188 \pm 0.042$ |
| 0.86 | $1.522 \pm 0.057$ | $1.175 \pm 0.046$ |

attributed to a statistical uncertainty that would be reduced by computing substantially more numerous random paths). When, however, the source and detector are placed in a region of strong gradients, significant discrepancies occur.[‖] Furthermore, contrary to what was hoped, implementing the semi-analytical time-stepping scheme of Yee and Wilson (2007) to obviate the necessity of intervening to reset excessively large velocities (here defined as velocity fluctuations exceeding six times the local standard deviation) did not restore forward–backward equivalence. We return to this subject in section 5.2.

## 5. Performance relative to Oklahoma City field trial IOP9 release 2

In June–July 2003 tracer experiments were performed in central Oklahoma City (Allwine and Leach, 2007); Flaherty *et al.,* 2007; and companion papers). Here we focus on Intensive Observations Period IOP9 release 2, when sulphur hexafluoride was released continuously from 0600 to 0630 Local Standard Time, LST (27 June) from a near-ground point source on Park Avenue (latitude 35.4687°N, longitude 97.5156°W). The source

[‖] Additional forward–backward consistency tests were performed in the flow field computed by Bourdin and Wilson (2008) for diagonal flow across a square plot surrounded on all sides by a porous windbreak (the experimental flow is described by Wilson and Flesch, 2003). These tests, which will be reported elsewhere, revealed substantially more serious inconsistency of forward and backward simulations than indicated by Table II for the MUST flow. Ratios $C_b/C_f$ that were both lower and higher than unity were found, and as an example (not necessarily the worst case) $C_b/C_f < 0.1$ for a source at plot centre and detector at the intersection of two shelter fences. Inhomogeneity of the Reynolds stress tensor is the underlying cause of this forward/backward asymmetry of the discretized Thomson model. A further comment on Lagrangian dispersion simulations in this flow field follows in the conclusions.



DOI: 10.1002/qj

strength was $Q = 2\,\mathrm{g\,s^{-1}}$, and winds blew from the south. We assume concentrations (provided by the NOAA Air Resources Laboratory Field Research Division, on the 'ARLFRD grid') averaged over 0615–0630 LST approximate the mean concentration that would occur under stationarity of both the meteorology and the source.

The urbanSTREAM grid covered a volume of 1934.25 m×3610.6 m×800.0 m in the $x$- (west–east), $y$- (south–north) and $z$- (vertical) directions respectively, covering the central business district of Oklahoma City with $98 \times 138 \times 68$ coordinate planes. The urbanSTREAM coordinate origin is defined to be the southwest corner of the domain, which in this case stood at (35.449959°N, 97.52694°W). Within this overall computational boundary lay a sub-domain within which buildings were explicitly resolved; its southwest corner stood at $(x,\ y) = (644.75,\ 1611.88)$ m and its northeast corner at $(x, y) = (1289.5,\ 2321.1)$ m. The source for IOP9r2, placed at $(x_{\mathrm{src}}, y_{\mathrm{src}}) = (1001.7,\ 2095.7)$ m, therefore lay about 1 km east and 2.1 km north of the southwest corner of the grid, and the grid lengths of the cell containing the source were $\Delta x, \Delta y, \Delta z = (8,\ 7,\ 3)$ m. Figure 4 displays a region of the city containing the source and (some of) the detectors; the source and the detectors were at height 1.9 m, within the lowest layer of cells of the urbanSTREAM grid. Vertical profiles $\sigma_w(z)$ of the standard deviation of vertical velocity are given in Figure 5 for three locations (at the source, and at detectors 65 and 84). Note the elevated peak in $\sigma_w$ broadly at or near the effective top of the urban canopy; the strong vertical gradients in $\sigma_w$ will have exerted a strong influence on trajectories.

The salient characteristic of a typical urban core is irregularity on a length-scale $L$ set by building dimensions and spacing. Until the plume from a source has expanded to have a cross-section $\ell \gg L$, its spatial distribution relative to a Cartesian coordinate system is irregular, and plotting measured or modelled concentrations on vertical profiles or horizontal transects does not give rise to orderly curves that can be understood in terms of familiar paradigms, e.g. mean ground-level concentration due to a continuous ground-level point source decreasing monotonically with increasing height or with downstream distance ($C_0 \propto x^{-2}$, e.g. Batchelor, 1964). One mundane consequence is that there is little or nothing to be gained by ordering information that way, and the approach taken in this section is to compare modelled and measured concentrations on a log–log scatter diagram.

The tracer source for IOP9r2 was near ground level (i.e. 1.9 m), in the immediate lee (1.6 m from the wall) of a tall building on Park Avenue (Figure 1 in Flaherty *et al.,* 2007). Consequently the plume was unlike what would be seen on open terrain. Inspection of trajectories showed that most particles climbed up the wall of the building in a recirculation eddy, until released into the wind stream passing over its top (cf. Figure 2 in Christen *et al.,* 2003). Figure 6 and Table III indicate the reasonably good agreement between the forward Lagrangian stochastic simulation ($\mu = 0.05$) and the corresponding observations in this extremely complex flow (for which, surely, the computed velocity field is imperfect). The modelled concentrations lie within a factor of two of the observations in nine of the

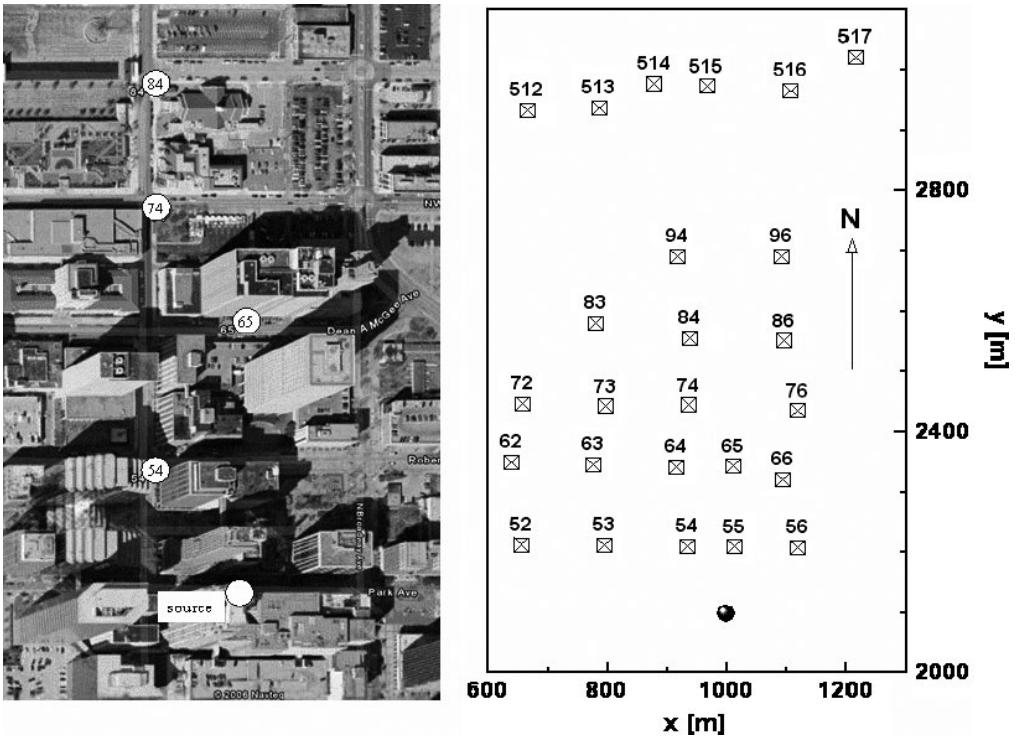


Figure 4. Oklahoma City, and layout of detectors with their positions on the urbanSTREAM grid. The streamwise ($y$) distance from the source to detector 74 is about 350 m. (The diagrams are not drawn to the same scale.)



DOI: 10.1002/qj

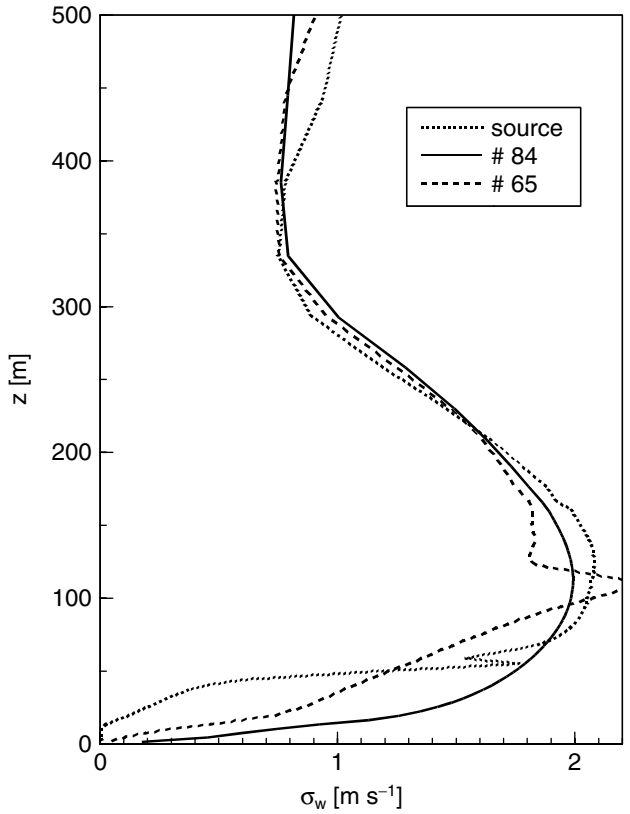


Figure 5. Examples of urbanSTREAM's computed profiles of the standard deviation of vertical velocity, for the IOP9r2 flow. Locations of the profiles can see seen in Figure 4, and kinks in the profiles reflect the influence of nearby building towers.

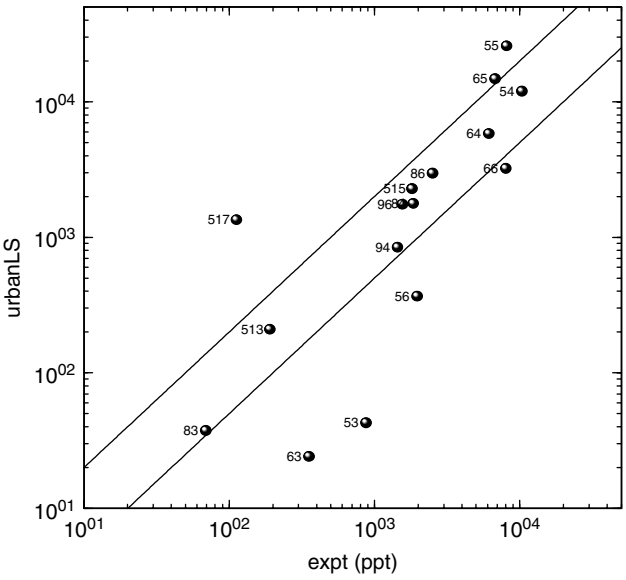


Figure 6. Comparison of observed and modelled mean concentrations (ppt) for IOP9 release 2 (Oklahoma City, Joint Urban 2003). Lines denote model/observation ratios of (1/2 and 2). Forward simulation, first-order LS (1f).

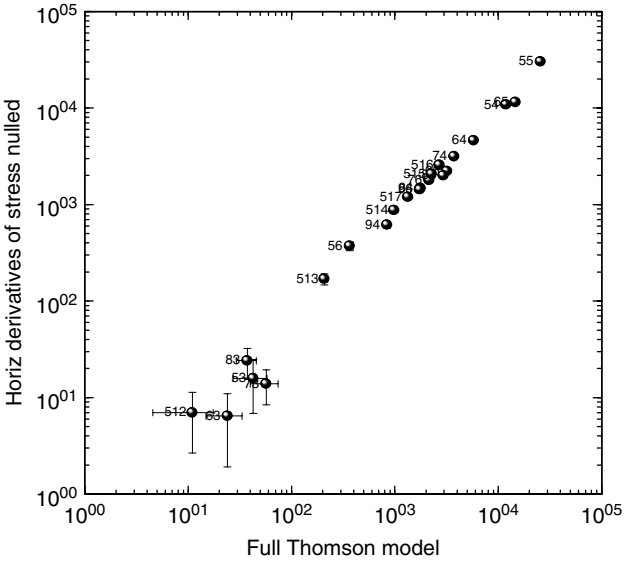


Figure 7. Computed concentrations (ppt) for IOP9r2, with terms in the Thomson LS model that involve horizontal derivatives of the stress tensor suppressed (however, velocity covariance is retained; $C_0 = 4.8$). Error bars give the standard error; these are hidden by symbols in most cases.

total of sixteen cases** (FAC2 = 0.56; Table III) for which observed concentration was non-zero, an outcome which compares reasonably favourably with the FAC2 = 0.67 obtained by Milliez and Carissimo (2007) from Eulerian ($k - \epsilon$) simulations of the MUST field trials in a simpler (periodic) 'urban' setting. (Milliez and Carissimo do not specify the value they used for the turbulent Schmidt number which, like other constants of the closure scheme, may have been tuned for optimal agreement with MUST.) We may also compare the present results with a somewhat similar study by Carvalho *et al.* (2002) wherein the same Lagrangian stochastic model, driven by meteorological fields from the mesoscale weather model RAMS, computed the pattern of ground-level concentration over a region (very roughly 150×150 km) of the Rhine Valley. Carvalho *et al.* compared their simulated concentration field with the measured concentrations at ten locations that had reported non-zero concentrations and their best results, obtained when RAMS was run at 4 km horizontal resolution, gave a FAC2 of 0.14–0.57, depending on specific assumptions in regard to ABL depth and turbulence profiles.

**The corresponding *backward* first-order LS simulation, from a total of sixteen of the IOP9r2 detectors, scored FAC2 = 8/16. An Eulerian simulation, with the turbulent Schmidt number specified as $S_c = 0.63$, yielded FAC2 = 10/16 (E. Yee, personal communication, 2006).

### 5.1. Consequences of simplifying the LS model

When given horizontally varying fields of velocity statistics, one may be tempted to invoke 'local homogeneity', wherein terms in the well-mixed Thomson model that involve *horizontal* derivatives of (any) velocity covariance are dropped. Figure 7 shows that the impact of that simplification upon the computed concentration field for IOP9 is very modest, the FAC2 score remaining high at FAC2 = 8/16 = 0.5.

However, if terms involving vertical derivatives of stress are also dropped, model performance is poor



DOI: 10.1002/qj

Table III. Comparison of observed mean concentration (0615–0630, [ppt]) during IOP9 release 2, and the outcome of LS simulations (1f, 1b). Both LS simulations used $dt/T_L = 0.05$. Forward simulations have $19 \times 80\,000$ paths, and backward simulations have $19 \times 102\,400$ paths backward from each of a subset of 16 detectors that had reported non-zero concentration.

| Location | Observed | 1f (st.err.) | 1b (st.err.) | 1f/Obs | 1b/Obs |
|---|---|---|---|---|---|
| 52 | – | 0 (0) | – | – | – |
| 53 | 881 | 43 (15) | 0 (0) | 0.05 | 0.00 |
| 54 | 10399 | 11911 (397) | 7677 (469) | 1.15 | 0.74 |
| 55 | 8164 | 25694 (257) | 35430 (951) | 3.15 | 4.34 |
| 56 | 1980 | 366 (32) | 498 (115) | 0.19 | 0.25 |
| 62 | – | 0 (0) | – | – | – |
| 63 | 356 | 24 (9) | 23 (15) | 0.07 | 0.06 |
| 64 | 6167 | 5792 (129) | 7502 (442) | 0.94 | 1.22 |
| 65 | 6809 | 14705 (207) | 12201 (520) | 2.16 | 1.79 |
| 66 | 8070 | 3205 (127) | 3952 (288) | 0.40 | 0.49 |
| 72 | – | 0 (0) | – | – | – |
| 73 | – | 57 (17) | – | – | – |
| 74 | – | 3750 (127) | – | – | – |
| 76 | – | 2149 (99) | – | – | – |
| 83 | 70 | 37 (8) | 57 (44) | 0.54 | 0.82 |
| 84 | 1860 | 1767 (67) | 3366 (347) | 0.95 | 1.81 |
| 86 | 2525 | 2955 (100) | 4325 (280) | 1.17 | 1.71 |
| 94 | 1450 | 840 (50) | 1936 (265) | 0.58 | 1.33 |
| 96 | 1565 | 1743 (56) | 3776 (236) | 1.11 | 2.41 |
| 512 | – | 11 (6) | – | – | – |
| 513 | 192 | 208 (16) | 276(92) | 1.09 | 1.44 |
| 514 | – | 983 (43) | – | – | – |
| 515 | 1826 | 2270 (80) | 878 (149) | 1.24 | 0.48 |
| 516 | – | 2695 (94) | – | – | – |
| 517 | 113 | 1340 (51) | 994 (184) | 11.9 | 8.79 |

(Figure 8), indeed FAC2 = 0. This is presumably attributable to the spurious neglect of the drift correction term $\partial\sigma_w^2/\partial z$ in the Langevin equation for vertical velocity, e.g. Wilson and Sawford (1996), whose Equation (12) gives that Langevin equation for the case of a 1D model for horizontally homogeneous Gaussian turbulence. Referring to Figure 5, we see that this term would have the effect of pushing particles that are near ground towards larger heights, so that its neglect could be expected to increase ground-level concentrations.

Another tempting simplification of the full 3D Thomson model is to neglect velocity covariance, i.e. set the off-diagonal terms in the stress tensor to zero. Again, quite a number of terms could accordingly be dropped from the generalized Langevin equation if one wished to reduce the computational burden. A simulation (not shown) proved that neglect of the $\overline{u'v'}$ covariance has negligible impact on the simulation (FAC2 remains at 9/16). However Figure 9 shows that if the covariance of vertical velocity with the horizontal velocities (also) is neglected, the FAC2 score is negatively impacted, dropping from the reference value of 9/16 (covariances retained, $C_0 = 4.8$ i.e. the 'calibration value') to 7/16 (covariance neglected, $C_0$ accordingly reduce to $C_0 = 3.59$) or more steeply to 6/16 if that adjustment of $C_0$ is not made. This is perhaps the first indication that retaining the velocity covariance is advantageous for the prediction of dispersion in a complex flow.

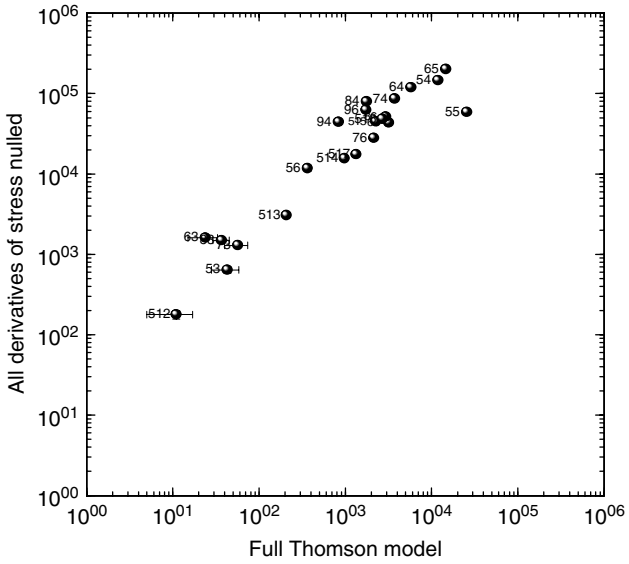


Figure 8. Computed concentrations (ppt) for IOP9r2, with terms in the Thomson LS model that involve horizontal *or vertical* derivatives of the stress tensor suppressed (however, velocity covariance is retained; $C_0 = 4.8$). Error bars give the standard error; these are hidden by symbols in most cases.



DOI: 10.1002/qj

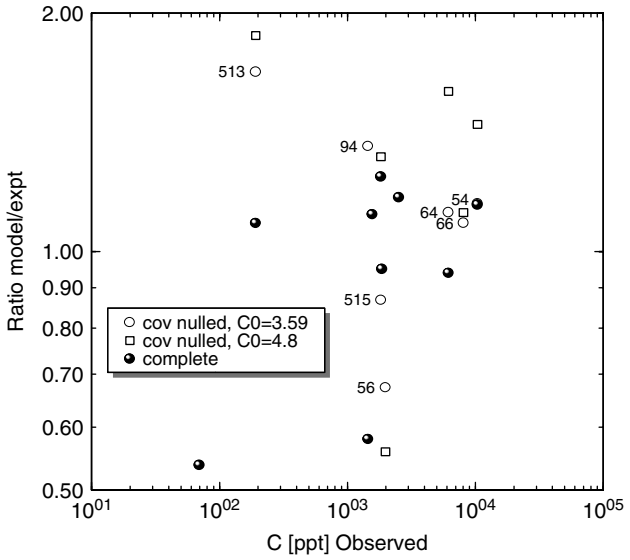


Figure 9. Impact of neglecting velocity covariance on LS model performance for IOP9r2. As shown earlier, if covariance is important in regard to vertical spread, then its neglect might be expected to be compensated to some degree by the proper optimization of $C_0$, arguably as $C_0 = 3.59$.

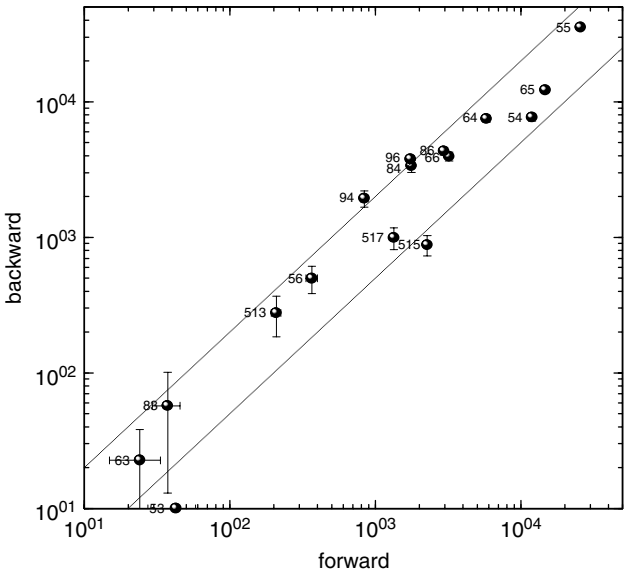


Figure 10. Comparison of computed concentrations (ppt) from forward and backward first-order LS simulations of IOP9 release 2 (Oklahoma City, Joint Urban 2003), showing all 16 stations that reported non-zero concentration. Error bars give the standard error; these are hidden by symbols in most cases.

Finally, what if one adopts a *one-dimensional* LS model, that is, if one neglects entirely the horizontal velocity fluctuations? In that case the LS model reduces to the unique well-mixed model for vertically inhomogeneous Gaussian turbulence and, according to what has been seen earlier, we should specify $C_0 = 3.59$. The temptation to drop $u', v'$ stemmed from a speculation that differential advection in the highly complex mean flow field might render the contribution of the horizontal velocity fluctuations unimportant. However when put to the test, such a simulation produced an unrealistically narrow plume and very poor agreement with the observations; station 55, seriously overpredicted by the full model (Table III) was the only prediction within a factor of two of observation, thus FAC2 $= 1/16$.

The point of this section, then, is to indicate the need for caution if adopting a heuristic LS model rather than the well-mixed model. While it is true that one might be able to compensate to some extent for the choice of a simpler model by adjusting the value of $C_0$, in doing so one departs from the most rational approach. A final point worth making very emphatically is that if the driving velocity field is rendered horizontally-homogeneous by application of an area-average encompassing all unoccupied cells on each given horizontal plane, the LS model scores a far poorer FAC2=2/16 (in lieu of 9/16); accounting for the horizontal inhomogeneity of the flow is crucial.

### 5.2. Comparison: Forward and backward simulations

Backward simulations were performed from all sixteen detectors that had reported non-zero concentration during IOP9r2, namely numbers 53–56, 63–66, 83, 84, 86, 94, 96, 513, 515, 517. Figure 10 indicates that backward and forward simulations, identical as regards all physical and numerical parameters (including the time step $\mu = 0.05$), produce concentration estimates at the IOP9r2 detectors that, while very similar, differ by a margin much greater than the standard error (this is seen most clearly in Table III).

Forwards–backwards equivalence is an assured property of the infinitesimal-d$t$ (i.e. continuous) Lagrangian models. By the evidence above (also section 4.2), it is not upheld in the present discrete implementation. Possible mechanisms to break the symmetry include: (a) discreteness of the velocity statistics, implying discontinuities from cell to cell, (b) reflection off building walls, and (c) reflection off ground.

If (c) were relevant, the f/b discrepancy should be observable even in LS models for which velocity statistics are given as a continuous function of particle position. Relative to standard error, however, differences in the outcomes of test forward and backward simulations (time step $\mathrm{d}t/T_L = 0.01$) of a source in the horizontally uniform surface layer (whose flow properties were specified as continuous functions of height) were insignificant. Thus the origin of the forward/backward non-equivalence lies in (a) or (b). Regarding wall reflection, 'nudging' the reflected particles to the exact distance $\ell_n$ (set to $\ell_n = 1$ m for the IOP9r2 simulations) outside a wall must result in a small-scale non-uniformity of the computed concentration field, and in that case proximity of a detector or source to a wall might modulate the degree of forward/backward inconsistency.

To eliminate the possible influence of wall reflection, matched forward and backward simulations were performed for a (hypothetical) case where the source and the detector were placed far from the city core, i.e. outside the sub-domain of resolved buildings and the possibility of proximate walls. In this case the source and detector



DOI: 10.1002/qj

were given identical volumes (i.e. volume source rather than point source, with the volume of source and detector equal). For these simulations $\mathrm{d}t/T_L = 0.1$, with other details the same as above.

The (forward) source was centred at $x = 1001.7$, $y = 800.0$, $z = 10.0\,\mathrm{m}$, and $(19\times16\,000)$ particles were released uniformly over a surrounding volume whose half-spans were $(50 \times 50 \times 5)\,\mathrm{m}$. The (forward) detector was centred at $x = 1001.7$, $y = 3000.0$, $z = 10.0\,\mathrm{m}$, and had the same half-spans $(50 \times 50 \times 5)\,\mathrm{m}$. Forward and backward simulations, identical in all respects but for exchange of source and detector, resulted in outcomes: $C^{\mathrm{f}} = 419 \pm 18\,\mathrm{ppt}$ versus $C^{\mathrm{b}} = 254 \pm 12\,\mathrm{ppt}$, where the specified uncertainty is the standard error, and where (for both simulations) the source strength, integrated over its volume, was $Q = 2.0\,\mathrm{g\,s^{-1}}$. The outcomes of these carefully matched forward and backward simulations differ significantly from each other. It seems most likely that mechanism (a), the discreteness of the velocity statistics, is causing the non-equivalence of forward and backward simulations.

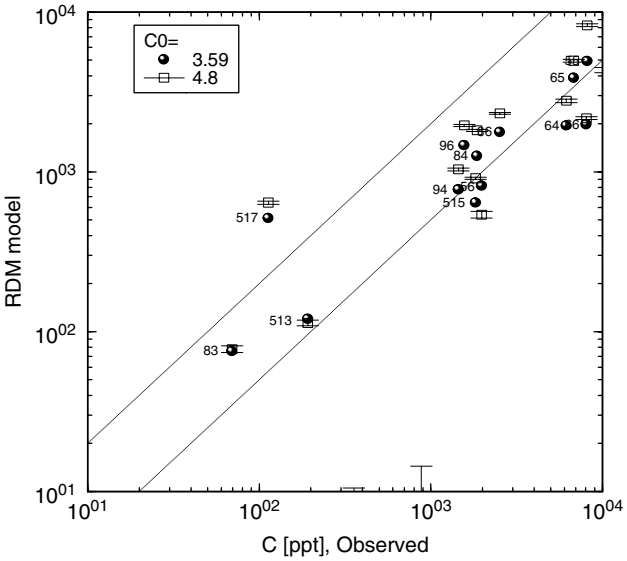


Figure 11. Performance of the forward Random Displacement Model (0f) for IOP9 release 2, according to two choices of the Kolmogorov constant $C_0$.

### 5.3. Performance of Random Displacement Model

The Random Displacement Model (RDM)

$$\mathrm{d}X_i = \left(\overline{u}_i + \frac{\partial K_{(i)}}{\partial x_{(i)}}\right)\mathrm{d}t + \sqrt{2K_{(i)}}\;\mathrm{d}\xi_{(i)} \qquad (25)$$

(e.g. Näslund *et al.,* 1994) is equivalent to an eddy diffusion treatment, and generally considered a satisfactory treatment in the far field of sources. (As earlier, a bracketed index, $(i)$, signifies summation is not implied; $\mathrm{d}\xi_i$ represents a Gaussian random variate with $\langle \mathrm{d}\xi_i \rangle = 0$ and $\langle (\mathrm{d}\xi_i)^2 \rangle = \mathrm{d}t$.) In this model the eddy diffusivity is anisotropic but diagonal, and we have evaluated it (following Taylor, 1921) as

$$K_{(i)} = \sigma_{(i)}^2\, T_L\,, \qquad (26)$$

where $\sigma_{(i)}$ is the velocity standard deviation along coordinate direction $i$ and as earlier $T_L = 2\sigma_w^2/(C_0\epsilon)$. For backward simulations $\overline{u}_i$ is reversed in sign (with $\mathrm{d}t > 0$ according to our program design), but the drift term $\partial K_{(i)}/\partial x_{(i)}$ is *not* reversed. Following the recommendation of Wilson and Yee (2007), the time step for the RDM has here been subjected to the limitation

$$\mathrm{d}t = \mu\, \min\left[\tau_v,\, \tau_h\right], \quad (\mu \ll 1)\,, \qquad (27)$$

where the inhomogeneity time-scale $\tau_h$ was given earlier (24), and a second (heuristic) limit

$$\tau_v = \frac{2S_c z}{k_v}\left(\overline{u'w'}^2 + \overline{v'w'}^2\right)^{-1/4} \qquad (28)$$

is introduced to ensure that the root mean square step length $\sqrt{2K\,\mathrm{d}t}$ is small enough to satisfy

$$\sqrt{2K\,\mathrm{d}t}\;\frac{1}{K}\;\frac{\partial K}{\partial z} \ll 1\,. \qquad (29)$$

For consistency with first-order LS simulations, IOP9r2 simulations with the RDM also used $\mu = 0.05$.

Figure 11 gives the predictions of the RDM for two choices of $C_0$. In the case that $C_0 = 3.59$, which (we would argue) is the most reasonable choice, the RDM scores FAC2 $= 8/16$, although in principle it ought to match the FAC2 $= 10/16$ scored by the Eulerian solution mentioned earlier. A slightly better FAC2 $= 9/16$ is attained with $C_0 = 4.8$, a choice (however) that cannot be defended.

This section has established that for the Oklahoma City IOP9r2 far-field dispersion problem, performances of the random displacement model and the more complex Langevin model are very similar (FAC2s of 8 and 9 respectively). This should not be surprising. The argument in favour of the Langevin treatment is its greater fidelity to the underlying process, for following Thomson (1987) one explicitly crafts the generalized Langevin equation to reflect available information on the velocity statistics.

## 6. Conclusion

Whereas, in the interests of computational speed, others (e.g. Diehl *et al.,* 2007) have explored the use of simplified, heuristic Lagrangian stochastic models to compute urban dispersion, our aim here has been to document the performance of Thomson's well-mixed model. Although urban velocity statistics are not (in general) Gaussian, their deviation from Gaussianity is neither universal, nor in any generalizable sense known. Therefore the adoption of Thomson's LS model, based as it is on the assumption of Gaussian velocity PDFs, should not be the most serious of the causes of loss of accuracy, particularly if we consider urban flows that are not too strongly affected by buoyancy.



DOI: 10.1002/qj

Lagrangian simulations of a full-scale urban dispersion experiment were performed using Thomson's model with a time step sufficiently small ($\mathrm{d}t/T_L \leq 0.05$) to assure the results are effectively time-step-independent. Without tuning of physical (e.g. $C_0$) or numerical (e.g. $\mathrm{d}t/T_L$) parameters away from reference values known to be appropriate (or optimal) in the very simplest regime of atmospheric turbulence (horizontally uniform and neutrally stratified surface layer), and on the basis of an imperfect computed field of velocity statistics, Thomson's LS model has given reasonably accurate predictions (FAC2$>$ 50%) at street scale of the field of mean concentration due to a point source, in a flow (urban core) whose complexity can scarcely be exceeded.[††] Eulerian calculations (as described by Keats *et al.,* 2007) provide comparably good performance, which is not surprising because, given that the source was near ground, all the present observations can be regarded as having been made in the far field.

The most interesting and surprising of our findings is that, while forward and backward simulations provide comparable answers, they are not exactly equivalent. This has to be interpreted as owing to discretization error (the corresponding continuous models are known to be symmetric), and specifically the cause is abrupt spatial changes in the Reynolds stress tensor. Reflection off building walls does play an influential role in this dispersion problem; e.g. if absorption (rather than reflection) is imposed on walls, the predicted concentration (averaged over the sixteen detectors of IOP9r2) falls to 41% of its reference value with reflection. However the reasonable agreement of LS simulation (with wall reflection) and observations suggests that, while not rigorous, the wall reflection scheme used is acceptable.

Non-equivalence of forward and backward simulations is of particular concern in the context of (potentially) applying the backward Lagrangian method for 'inverse dispersion' calculations, such as outlined by Flesch *et al.* (1995), in flows disturbed by obstacles such as barns, reservoirs, etc. Although with care in instrument placement, useful results may be obtained while *neglecting* horizontal variability of velocity statistics (e.g. Flesch *et al.* (2009) who quantified ammonia emissions from dairy farms on the basis of measured downwind concentrations), one would hope to be able to achieve higher fidelity by the strategy of supplying the Lagrangian model a computed estimate of the, actually, *disturbed* statistics. An obvious question is whether interpolating velocity statistics from the flow grid to particle position might substantially moderate or even eliminate the forwards–backwards non-equivalence noted above–for urbanLS employs no such interpolation. We have addressed this question in a preliminary way with further forward- and backward-dispersion simulations in the windbreak flow field computed by Bourdin and Wilson (2008), arbitrarily implementing an inverse-distance-weighted interpolation of flow statistics (and the coefficients of the Langevin equation, i.e. the $T$s) to the particle position. (The interpolation used information from up to eight neighbouring nodes.) This refinement resulted in but modest changes to computed concentration fields (consistent with a similar report by Wilson and Yee, 2000), whereas dramatic change would have been needed, if this were to be the explanation for, and avenue to eliminate, forward–backward inconsistency of Lagrangian simulations.

[††]Forward Lagrangian simulation of Oklahoma City run IOP9r2 (Figure 6, $19 \times 80\,000$ paths) occupied about 3 hours on a workstation (2MB RAM; AMD Athlon Dual Core Processor 4800+ with CPU speed 2494.025 MHz). However, the inherent parallelism in the forward (or, backward) LS model can be easily exploited by running each sub-ensemble of particles on a different processor of a massively parallel computer.

## Acknowledgements

The authors acknowledge support from the Chemical Biological Radiological Nuclear Research and Technology Initiative (CRTI) Program under project number CRTI-02-0093RD, and thank the unknown reviewers for their helpful remarks.

## References

Allwine J, Leach M. 2007. Editorial. *J. Appl. Meteorol. Climatol.* **46**: 2017–2018. Special issue on results from the Joint Urban 2003 atmospheric dispersion study.

Barad ML. 1958. Project Prairie Grass, a field program in diffusion (Vol. 2). Geophysical Research Papers 3, Geophysical Research Papers No. 59, TR-58-235(II), Air Force Cambridge Research Center: Cambridge, Mass, USA.

Batchelor GK. 1964. Diffusion from sources in a turbulent boundary layer. *Archiwum Mechaniki Stosowanej* **3**: 661–670.

Borrego C, Tchepel O, Costa AM, Amorim JH, Miranda AI. 2003. Emission and dispersion modelling of Lisbon air quality at local scale. *Atmos. Environ.* **37**: 5197–5205.

Bourdin P, Wilson JD. 2008. Windbreak aerodynamics: Is CFD Reliable? *Boundary-Layer Meteorol.* **126**: 181–208. DOI: 10.1007/s10546-007-9229-y.

Carvalho JC, Anfossi D, Trini Castelli S, Degrazia GA. 2002. Application of a model system for the study of transport and diffusion of complex terrain to the TRACT experiment. *Atmos. Environ.* **36**: 1147–1161.

Christen A, Vogt R, Rotach MW. 2003. 'Profile measurements of selected turbulence parameters over different urban surfaces'. *4th International Conference on Urban Air Quality, Prague 408–411*. http://pages.unibas.ch/geo/mcr/Crew/AC/pdfs/prague_christen.pdf.

Diehl SR, Burrows DA, Hendricks EA, Keith R. 2007. Modeling turbulent flow in an urban central business district. *J. Appl. Meteorol. Climatol.* **46**: 2180–2191.

Durbin PA. 1983. 'Stochastic differential equations and turbulent dispersion'. Reference publication 1103, NASA: Glenn Research Center: Ohio, USA.

Flaherty JE, Lamb B, Allwine KJ, Allwine E. 2007. Vertical tracer concentration profiles measured during the Joint Urban 2003 dispersion study. *J. Appl. Meteorol. Climatol.* **46**: 2019–2037.

Flesch TK, Wilson JD. 1992. A two-dimensional trajectory-simulation model for non-Gaussian, inhomogeneous turbulence within plant canopies. *Boundary-Layer Meteorol.* **61**: 349–374.

Flesch TK, Wilson JD, Yee E. 1995. Backward-time Lagrangian stochastic dispersion models, and their application to estimate gaseous emissions. *J. Appl. Meteorol.* **34**: 1320–1332.

Flesch TK, Harper LA, Powell JM, Wilson JD. 2009. Inverse-dispersion calculation of ammonia emissions from Wisconsin dairy farms. *Trans. ASABE* **52**: 253–265.

Gardiner CW. 2004. Handbook of Stochastic Methods for Physics, Chemistry and the Natural Sciences. Springer: Berlin.

Haugen DA. (ed.) 1959. Project Prairie Grass, a field program in diffusion. Geophysical Research Papers No. 59, Vol. III, AFCRC-TR-58-235. Air Force Cambridge Research Center: Cambridge, Mass, USA.

Hilderman T, Chong R. 2007. 'A laboratory study of momentum and passive scalar transport and diffusion within and above a model urban canopy'. DRDC Suffield CR 2008-025, Defence R&D Canada: Suffield, Ralston, Alberta.

Kaplan H, Dinar N. 1996. A Lagrangian dispersion model for calculating concentration distribution within a built-up domain. *Atmos. Environ.* **30**: 4197–4207.

Keats A, Yee E, Lien F-S. 2007. Bayesian inference for source determination with applications to a complex urban environment. *Atmos. Environ.* **41**: 465–479.

Lanzani G, Tamponi M. 1995. A microscale Lagrangian particle model for the dispersion of primary pollutants in a street canyon. Sensitivity analyses and first validation trials. *Atmos. Environ.* **29**: 3465–3475.

Lee RL, Näslund E. 1998. Lagrangian stochastic particle model simulations of turbulent dispersion around buildings. *Atmos. Environ.* **32**: 665–672.

Leuzzi G, Monti P. 1998. Particle trajectory simulation of dispersion aound a building. *Atmos. Environ.* **32**: 203–214.

Lien F-S, Yee E. 2004. Numerical modelling of the turbulent flow developing within and over a 3-D building array, Part I: A high-resolution Reynolds-averaged Navier–Stokes approach. *Boundary-Layer Meteorol.* **112**: 427–466.

Lien F-S, Ji H, Yee E. 2007. 'Parallelization of an urban microscale flow model (urbanSTREAM): Component 1 of CRTI Project 02-0093RD'. DRDC Suffield CR 2008-025, Defence R&D Canada: Suffield, Ralston, Alberta.

Mayer D, Reiczigel J, Rubel F. 2008. A Lagrangian particle model to predict the airborne spread of foot-and-mouth disease virus. *Atmos. Environ.* **42**: 466–479.

Milliez M, Carissimo B. 2007. Numerical simulations of pollutant dispersion in an idealized urban area, for different meteorological conditions. *Boundary-Layer Meteorol.* **122**: 321–342.

Näslund E, Rodean HC, Nasstrom JS. 1994. A comparison between two stochastic diffusion models in a complex three-dimensional flow *Boundary-Layer Meteorol.* **67**: 369–384.

Rotach MW. 2001. Simulation of urban-scale dispersion using a Lagrangian stochastic dispersion model. *Boundary-Layer Meteorol.* **99**: 379–410.

Rotach MW, Gryning S-E, Batchvarova E, Christen A, Vogt R. 2004. Pollutant dispersion close to an urban surface – The BUBBLE tracer experiment. *Meteorol. Atmos. Phys.* **87**: 39–56.

Santiago JL, Martin F. 2008. SLP-2D: A new Lagrangian particle model to simulate pollutant dispersion in street canyons. *Atmos. Environ.* **42**: 3927–3936.

Sawford BL. 1999. Rotation of trajectories in Lagrangian stochastic models of turbulent dispersion. *Boundary-Layer Meteorol.* **93**: 411–424.

Sawford BL. 2001. 'Project Prairie Grass – A classic atmospheric dispersion experiment revisited'. In *Proceedings of 14th Australian Fluid Mech. Conference, Adelaide, Australia*.

Sawford BL, Guest FM. 1988. 'Uniqueness and universality of Lagrangian stochastic models of turbulent dispersion'. Pp 96–99 in *Preprints of 8th AMS Symposium on Turbulence and Diffusion, San Diego, CA. Amer. Meteorol. Soc: Boston*.

Taylor GI. 1921. Diffusion by continuous movements. *Proc. London Math. Soc.* series 2, **A20**: 196–211.

Tennekes H. 1979. The exponential Lagrangian correlation function and turbulent diffusion in the inertial subrange. *Atmos. Env.* **13**: 1565–1567.

Thomson DJ. 1987. Criteria for the selection of stochastic models of particle trajectories in turbulent flows. *J. Fluid Mech.* **180**: 529–556.

Tinarelli G, Brusasca G, Oldrini O, Anfossi D, Trini Castelli S, Moussafir J. 2007. Micro-Swift-Spray (MSS): A new modelling system for the simulation of dispersion at microscale. General description and validation. Pp 449–458 in *Air Pollution Modeling and Its Application XVII*. Springer: Berlin.

Wang B-C, Yee E, Lien F-S. 2009. Numerical study of dispersing pollutant clouds in a built-up environment. *Int. J. Heat Fluid Flow* **30**: 3–19.

Wilson JD. 1982a. An approximate analytical solution to the diffusion equation for short-range dispersion from a continuous ground-level source. *Boundary-Layer Meteorol.* **23**: 85–103.

Wilson JD. 1982b. Turbulent dispersion in the atmospheric surface layer. *Boundary-Layer Meteorol.* **22**: 399–420.

Wilson JD. 2008. Monin-Obukhov functions for standard deviations of velocity. *Boundary-Layer Meteorol.* **129**: 353–369.

Wilson JD, Flesch TK. 1997. Trajectory curvature as a selection criterion for valid Lagrangian stochastic models. *Boundary-Layer Meteorol.* **84**: 411–425.

Wilson JD, Flesch TK. 2003. Wind measurements in a square plot enclosed by a shelter fence. *Boundary-Layer Meteorol.* **109**: 191–224.

Wilson JD, Sawford BL. 1996. Lagrangian stochastic models for trajectories in the turbulent atmosphere. *Boundary-Layer Meteorol.* **78**: 191–210.

Wilson JD, Yee E. 2000. Wind transport in an idealised urban canopy. Preprints, 3rd Symposium on the Urban Environment, 40–41, American Meteorological Society.

Wilson JD, Yee E. 2007. A critical examination of the random displacement model of turbulent dispersion. *Boundary-Layer Meteorol.* **125**: 399–416.

Wilson JD, Thurtell GW, Kidd GE. 1981. Numerical simulation of particle trajectories in inhomogeneous turbulence. III. Comparison of predictions with experimental data for the atmospheric surface layer. *Boundary-Layer Meteorol.* **21**: 443–463.

Wilson JD, Ferrandino FJ, Thurtell GW. 1989. A relationship between deposition velocity and trajectory reflection probability for use in stochastic Lagrangian dispersion models. *Agric. Forest Meteorol.* **47**: 139–154.

Wilson JD, Flesch TK, Swaters GE. 1993. Dispersion in sheared Gaussian homogeneous turbulence. *Boundary-Layer Meteorol.* **62**: 281–290.

Wilson JD, Flesch TK, Harper LA. 2001. Micro-meteorological methods for estimating surface exchange with a disturbed windflow. *Agric. Forest Meteorol.* **107**: 207–225.

Yee E, Biltoft CA. 2004. Concentration fluctuation measurements in a plume dispersing through a regular array of obstacles. *Boundary-Layer Meteorol.* **111**: 363–415.

Yee E, Wilson JD. 2007. On the presence of instability in Lagrangian stochastic trajectory models, and a method for its cure. *Boundary-Layer Meteorol.* **122**: 243–261.

Yee E, Gailis RM, Hill A, Hilderman T, Kiel D. 2006. Comparison of wind-tunnel and water-channel simulations of plume dispersion through a large array of obstacles with a scaled field experiment. *Boundary-Layer Meteorol.* **121**: 389–432.

Yee E, Lien F-S, Ji H. 2007. 'Technical description of urban microscale modeling system: Component 1 of CRTI Project 02-0093RD'. DRDC Suffield TR 2007-067. Defence R&D Canada: DRDC Suffield, Ralston, Alberta.



DOI: 10.1002/qj

RMetS
Royal Meteorological Society

# Notes and Correspondence
# Erratum to 'Lagrangian simulation of wind transport in the urban environment'

J. D. Wilson,[a]* E. Yee,[b] N. Ek[c] and R. d'Amours[c]

[a]*Department of Earth and Atmospheric Sciences, University of Alberta, Edmonton, Alberta, Canada*
[b]*Defence R&D Canada–Suffield, Medicine Hat, Alberta, Canada*
[c]*Canadian Meteorological Centre, Dorval, Quebec, Canada*
*Correspondence to: J. D. Wilson, Department of Earth & Atmospheric Sciences, 1–26 Earth Sciences Building, University of Alberta, Edmonton, Alberta, Canada T6G 2E3. E-mail: jaydee.uu@ualberta.ca

**The above article was originally published on Early View on 28 July 2009, and subsequently in volume 135 (issue 643): 1586–1602; DOI:10.1002/qj.452.**

**A footnote on p 1595 alluded to a serious forwards/backwards inconsistency of the Lagrangian stochastic model, in calculations for hypothetical sources and detectors placed in a computed three-dimensional windbreak flow. It was subsequently discovered that a simple coding error in those particular Lagrangian simulations (i.e. only those pertaining specifically to the windbreak flow) had rendered the Reynolds stress gradients grossly wrong and that, with the error corrected, close forwards/backwards consistency obtains. The reported simulations of dispersion in urban-like flows, i.e. the main subject of the paper, were not subject to the error and are correct.** Copyright © 2010 Royal Meteorological Society

*Received 26 October 2009; Accepted 30 October 2009; Accepted ; Published online in Wiley InterScience*

*Citation:* Wilson JD, Yee E, Ek N, d'Amours R. 2010. Notes and Correspondence Erratum to 'Lagrangian simulation of wind transport in the urban environment'. *Q. J. R. Meteorol. Soc.* DOI:10.1002/qj.550